Spring 2018

Effects Of Air-Fuel Ratio And Operating Conditions On Particle Emissions From A Small Diesel Engine

Odinmma John-Paul Ofili
Bucknell University, ojpo001@bucknell.edu

I, Odinmma John-Paul Ofili, do grant permission for my thesis to be copied.

EFFECTS OF AIR-FUEL RATIO AND OPERATING CONDITIONS ON PARTICLE EMISSIONS FROM A SMALL DIESEL ENGINE

by

Odinmma John-Paul Ofili

A Thesis

Presented to the Faculty of
Bucknell University
In Partial Fulfillment of the Requirements for the Degree of
Master of Science in Mechanical Engineering

Approved:

Adviser

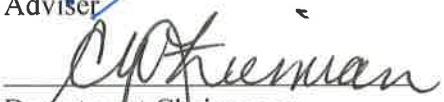

Department Chairperson

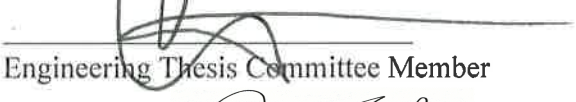

Engineering Thesis Committee Member

Engineering Thesis Committee Member

(Date: May 2018)

ACKNOWLEDGEMENTS

I would first off like to thank my wonderful parents for their love, support and guidance. I could never repay or thank them enough for being such a positive influence on my life, and always being there for me through thick and thin. I owe my brother Kenechukwu, for being a constant source of humor and for helping keep me on track.

I would like to extend my most heartfelt thanks to my sensational advisor, Dr. Indranil Brahma, for giving me the opportunity to work on this project. I am thankful to have worked with, and under him, he has left an indelible mark upon me and I will cherish his guidance for the foreseeable future. I know that I was not always the easiest person to work with and I am thankful to him for sticking with me. Completion of the work required for this thesis would have been impossible without his support and for that I am very grateful. I am also sincerely grateful to Dr. Christopher Mordaunt, and Dr. Peter Stryker for agreeing to be on my committee, offering their input on the scope of the project, and for their corrections and directions in the production of this thesis paper.

I must also thank Dr. Robert Midkiff, Gretchen Fegley and Dr. Laura Beninati, along with the Graduate Studies and Mechanical Engineering Departments for all their help with funding. I am thankful to Jennifer Figueroa and International Student Services for their help with working out the logistics of my immigration status.

Thanks to Tim Baker, Aaron Clarke, Dan Johnson, and Hugh Weber for sharing their immense wealth of experience and expertise, and for their help with machining and setting up the test cell. Thanks to Wade Hutchison for helping out with the data collections systems

and LabVIEW. Also, thanks to Matt Lamparter for helping out with the electrical systems.

I absolutely must thank my roommates and fellow graduate students, Zwelani Ngwenya and Chiedozie Ononuju for their helping hand even though they had their own theses and projects to work on. We started out on this journey together as roommates but now we have finished as brothers and for that I am sincerely grateful. I am also thankful to Chanda Singoyi and Eyuel Seyoum for being a source of support and for the fun times we had.

I would finally like to thank friends and family not mentioned here by name. Your support is part of the reason that I was able to complete the work required for this degree.

Contents

List of Figures

List of Tables

Nomenclature

Acronyms

FOV	Field of view
LFE	Laminar flow element
TDC	Top dead center

Greek Symbols

α	Angle of view
γ	The ratio of specific heats
ω	Rotational velocity
ρ	Density
θ	Crank angle

Roman Symbols

ΔP	Pressure drop across
$\dot{m}$	Mass flow rate
$\dot{V}$	Volumetric flow rate

a	Engine crank radius
B	Cylinder bore
C	Concentration
c	Specific heat
d	Sensor size
f	Focal length
k	Calibration factor
l	Connecting rod length
P	Pressure
Q	Heat released
R	Gas constant
r_c	Compression ratio
s	Length
T	Temperature
V	Cylinder volume

ABSTRACT

Automotive engineers typically increase the air-fuel ratio (AFR) of an engine to control the amount of smoke emitted, but it not quite known how this process affects particulate number (PN). In the work presented, AFR was independently varied to study its effects on PN. It was found that increasing the AFR reduced the concentrations of larger particles from 10^8 #/cm^3 to 10^6 #/cm^3 which is an effect observable as a reduction in smoke. However, the same increases in AFR only resulted in an energy specific PN change from 10^{15} #/kWh to 10^{14} #/kWh. The study was then extended to examine how different combinations of engine speed, torque and timing affected PN. It was found that variations in timing (17 ^{o}BTDC to 4 ^{o}BTDC), speed (2000RPM to 3000RPM), and load (0 ft-lb to 12 ft-lb) had negligible effects on the amount of normalized PN produced. A novel study was performed to investigate the contribution of lubricating oil on the PN, and it was found that changing the oil formulation changed the amount of nuclei (sub-20nm) mode particles produced, and running the engine with no oil substantially reduced the nuclei (sub-20nm) mode while leaving the large (over-20nm) particle mode unchanged.

Chapter 1

INTRODUCTION

1.1 Internal Combustion Engine

Engines are work-producing devices that have been designed to convert other forms of energy into mechanical energy. Combustion engines, otherwise known as heat engines, are a subset of these engines that convert chemical energy into mechanical energy by burning a fuel/working fluid [1].

Of these combustion engines, there are two kinds: the internal and external combustion engines. External combustion engines (ECE) use a working fluid that is separate from the combustion fluid (fuel) and is therefore heated externally, either through the engine wall or a heat exchanger, before being used to produce usable work. An example of an ECE is the steam engine. In the steam engine, the water is converted to steam by the heat generated by burning coal or some other solid fuel and the expansion of the water as it turns into steam acts on a piston to provide mechanical energy [1, 2].

On the other hand, internal combustion engines (ICE) use a working fluid that is also the fuel, which is heated internally within the engine as a part of its working cycle. ICEs can further be subdivided using the method of ignition as the classification criterion. Spark

ignition (SI) engines use an electrical spark to ignite the fuel [3]. Gasoline engines are an example of SI engines. Compression ignition (CI) engines use the inherent mechanical compressive energy of the engine to compress the fuel until it reaches a critical self-ignition point [4]. Diesel engines are an example of CI engines. It should be noted that stationary combustion engines like turbines are excluded from this classification.

Both kinds of ICE engines can be found in the majority of vehicles today. This includes smaller engines found in motorcycles and cars, to larger engines found in commercial trucks, all the way up to the monstrous marine engines used to power freight/transport ships. A trend that has been observed is that the engines found in larger applications are usually of the diesel CI kind. This is due to the fact that diesel engines are more efficient and offer more torque than an SI engine of a similar specification [5, 6] which is often beneficial in vehicles that will be run continuously over long periods of time.

Another difference between SI and CI engines can be found in the method of power regulation. SI engines regulate power by controlling the volumetric amount of airflow into, and through the engine using a throttle, while CI engines regulate power by controlling the amount of fuel injected into the cylinder [3, 4]. This difference in power regulation scheme causes higher pumping losses in SI engines, as part of the work produced must go into drawing the air past the throttle. This effect is not found in CI engines which results in CI engines operating with lower pumping losses and higher compression ratios, resulting in observable torque and efficiency increases.

Due to these increased compression ratios, CI engines are designed more robustly than an SI engine of similar specifications. This leads to the advantage of increased engine durability at the expense of weight savings and unit production cost. Therefore, with proper maintenance, a CI engine will last much longer than an SI engine before the necessity of replacement is imminent [6], which when coupled with the higher efficiency and torque makes CI engines the ideal choice for commercial/heavy-duty applications.

Historically, there has been a progression of what was focused on in the development of engines. Initially, the focus was on power. The Ford Model T had 20HP from the factory, which was average for the time. Only a few years later, the most powerful production cars prior to World War I had up to 400HP [7], which when compared with values around 1500HP [8] for today's cars, shows a tripling of power in just over a century. In addition, it has been shown that average power values have doubled in just the last 40 years [9]. This search for increasingly greater amounts of power has resulted in the need for higher levels of engine reliability to not only cope with the increased power, but also to make the vehicle cheaper and more convenient to run as it would break down less frequently [10].

Generally speaking, to increase the power from an engine, the amount of fuel combusted has to also be increased. This led to higher and higher levels of dangerous pollutants being produced as emissions were poorly understood at the time. The entirety of this thesis is based on the emissions from a diesel engine and the major pollutants are carbon monoxide (CO), unburned hydrocarbons (UHC), oxides of nitrogen (NO_x) and particle number (PN). These emissions are discussed in depth in Chapter 2. This is where the work presented in this study fits in as it aims to further understand these emissions from these small (< 11 hp [11]) diesel engines through experimental procedures.

1.2 Thesis Objectives

Particulate number (PN), in its most basic form, describes the specific (per unit basis, usually volume) number of particles that are produced from any combustion process. In the case of the proposed work, this combustion process will be from a diesel engine.

The goal of the work presented in this thesis is to investigate two major questions, listed below:

- How much PN and emissions are produced from the engine?

Testing will be performed at a range of engine parameters such as speed, torque, timing, etc. This is done as a first step in the determination of the total amount of PN produced from the engine during operation.

- What are the effects of operating conditions on these emissions, if any?

  The purpose of this question is to observe the changes in PN as engine operating conditions are changed. This is done to evaluate the effectiveness of the use of alternative operating points as a reductive measure in the emission of harmful substances from the engine.

The purpose of the work presented in this thesis is to determine how much PN is produced from the engine, and examine the effects of engine operating condition on the emitted PN. It should be noted that this is a comparative study; all the collected data will be compared to see if any important patterns or trends emerge.

Chapter 2

LITERATURE REVIEW

This chapter will go in-depth to define emissions, both in a regulated, and unregulated context and what makes up these emissions. It will outline the published work, what has and has not been done, the motivation for the proposed work, and how it aims to fill/fit into these gaps.

2.1 Regulated Engine Emissions

Combustion of fossil fuels has been historically associated with environmental issues. This is due to the fact that fossil fuels produce by-products that are harmful not only to the environment, but also to humans directly. This correlation between the combustion of fossil fuels has been known since the 40s when smog levels increased to record levels in the Los Angeles basin [12]. In 1952, it was shown that the smog problem resulted from the reactions between oxides of nitrogen and hydrocarbon compounds in the presence of sunlight [13].

Since this relationship has been established, measures have been taken to reduce the pollutant levels from the ICE. These include much stricter restrictions on the amount of

emissions that an ICE can produce if it is to be sold to the public. These restrictions have led to the production of some of the least polluting engines ever designed to date, and have led the academic community to look into fuels that burn more cleanly such as ultra low sulfur diesel and biodiesel [14].

Although engines of today are cleaner than they were in the past, they still produce substances that have negative effects on human health. Efforts have been made to eradicate these substances, but they cannot be completely eliminated as they are an intrinsic part of the chemistry of fossil fuel combustion. Gasoline and diesel fuels are hydrocarbon based and when they are combusted (oxidized) in nitrogen-rich air, they produce by-products which include oxides of carbon such as carbon monoxide (CO) and carbon dioxide (CO_2), unburned hydrocarbons (UHC), oxides of nitrogen (NO_x), and particulate matter (PM).

As SI engines regulate the amount of airflow going into the combustion chamber, there is an excess amount of fuel [3]. This is known as rich combustion due to the amount of fuel (gasoline) being more than the stoichiometric amount of oxidizer (air) [15]. This predisposes SI engines to producing more UHC and CO as there is not enough oxygen in the available air to fully oxidize the hydrocarbons present. On the other hand, CI engines regulate the amount of fuel injected into the combustion chamber [4] which results in an excess of air, otherwise known as lean combustion due to the amount of fuel (diesel) being stoichiometrically less than the amount of oxidizer (again, air) [15]. This causes CI engines to produce a lot more CO_2 as there is now enough oxygen to perform full oxidation. Carbon monoxide is dangerous due to its lack of color, odor and taste, and its low deadly dose level as 25 ppm over any one hour period is considered lethal [16]. Carbon dioxide has similar physical properties to CO, but has been found to have less of a direct effect on human health, and is an effective greenhouse gas, driving climate change and causing secondary affects on the environment [17].

The oxides of nitrogen or NO_x, is a group of compounds produced through secondary

reactions during combustion. It mainly consists of nitric oxide (NO), nitrous oxide (N_2O), and nitrogen dioxide (NO_2). Nitrous oxide is a non-toxic compound that is frequently used in surgery as an anesthetic and analgesic, and is also a potent greenhouse gas. When oxidized, nitrous oxide turns into nitric oxide, which is a classified hazardous free radical that is important in the chemical industry as an intermediate compound in various production processes. Nitrogen dioxide is extremely toxic to humans, even in low doses and has been know to affect the respiratory system, causing bronchitis and pneumonia. It has also been shown to negatively affect red blood cells which impedes the oxygen transport system of the body [18]. All NO_x compounds can cause acid rain (due to the formation of nitric acid) and smog, and are partially responsible for the depletion of the ozone layer as they are highly reactive with ozone [19].

Though SI engines utilize premixed combustion, they produce a fair amount of unburned hydrocarbons which goes contrary to the general rule that, in combustion devices employing premixed reactants, UHC levels are usually negligible [20]. This problem has been researched at great length and it is due to one of four reasons: flame quenching at the cylinder wall, crevice filling, fuel absorption and desorption into lubricating oil layers, and incomplete combustion due to poorly controlled transient operating parameters [21]. The UHC produced through these mechanisms escape primary combustion and end up contributing to the total UHC concentration observable in the exhaust.

In the case of CI engines, the diesel fuel is injected directly into the cylinder which causes the combustion mode to be primarily a diffusion (non-premixed) burn. There are two major mechanisms of UHC formation in diesel combustion: overleaning, which causes flame quenching due to excess air cooling, and undermixing, which causes flame quenching due to locally excess fuel [22, 23]. Diesel fuels have higher boiling points and molecular weights, which when combined with the heterogeneous nature of diesel combustion, gives rise to more complex UHC than gasoline combustion [23]. However, it should be noted

that due to the lean nature of CI combustion, diesel engines produce on average, less UHC than their gasoline counterparts [21, 23].

Particulate matter (PM), a complex mixture of organic and inorganic substances, describes all of the solid and liquid particles suspended in air which are either directly emitted as a result of the combustion process in the engine, or as a result of secondary processes that turns emitted gaseous/aerosolized pollutants into PM [24]. PM poses a health risk to humans, and has been known to cause inflammations stemming from foreign matter in the lungs, autoimmune responses to the matter in the lymphatic system, and oxidative stress due to reduced efficacy of the pulmonary system [25].

PM can be subdivided based on size into coarse, and fine particles which can vary over four orders of magnitude, from a few nanometers to tens of micrometers, with some overlap between 1μm and 2.5μm [26]. The coarse portion of the particles are formed through the mechanical break-up of larger solid particles. The amount of energy required to break up the larger particles increases with particle size which establishes the lower limit for the coarse fraction at about 1μm [26]. The fine particles are formed through nucleation; this is the initial process that occurs in the formation of a solid crystal from a liquid or vapor solution [27]. This nucleation mode is achieved either through coagulation, which is the combination of two particles into a larger one, or through the condensation of vapor molecules on existing particles. As with the coarse fraction, the fine fraction has an upper limit of roughly 1μm [26].

The emissions outlined in this section are all regulated in some manner. This means that there is a regulatory body, either at the federal, state, local level, or all three, which has placed upper limits on how much of these pollutants an engine can emit and still be considered safe for use by the general public. An example of such restrictions, as outlined by the US Environmental Protection Agency (EPA), for commercial heavy-duty [28] diesel engines is shown below in Table 2.1.

Table 2.1: US EPA & California Emission Standards for heavy-duty CI Engines (g/bhp-hr) [29].

Year	CO	HC[a]	HC[a]+NOx	NO_x	PM	
					General	Urban Bus
1974	40	-	16	-	-	
1979	25	1.5	10	-	-	
1985	15.5	1.3	-	10.7	-	
1987	15.5	1.3	-	10.7[d]	0.60[f]	
1988	15.5	1.3[b]	-	10.7[d]	0.60	
1990	15.5	1.3[b]	-	6.0	0.60	
1991	15.5	1.3[c]	-	5.0	0.25	0.25[g]
1993	15.5	1.3[c]	-	5.0	0.25	0.10
1994	15.5	1.3[c]	-	5.0	0.10	0.07
1996	15.5	1.3[c]	-	5.0[e]	0.10	0.05[h]
1998	15.5	1.3	-	4.0	0.10	0.05[h]
2004[j]	15.5	-	2.4[i]	-	0.10	0.05[h]
2007	15.5	0.14[k]	-	0.20[k]	0.01	
2015	15.5	0.14	-	0.02[l]	0.01	

a. NMHC for 2004 and later standards
b. For methanol-fueled engines, the standard is for total hydrocarbon equivalent (THCE).
c. California: NMHC = 1.2 g/bhp·hr, in addition to the THC limit.
d. California: NOx = 6.0 g/bhp·hr
e. California: Urban bus NOx = 4.0 g/bhp·hr
f. California only, no federal PM limit.
g. California standard 0.10 g/bhp·hr
h. In-use PM standard 0.07 g/bhp·hr
i. Alternative standard: NMHC+NOx = 2.5 g/bhp·hr and NMHC = 0.5 g/bhp·hr
j. Under the 1998 Consent Decrees, several manufacturers supplied 2004 compliant engines from October 2002.
k. NOx and NMHC standards were phased-in on a percent-of-sales basis: 50% in 2007-2009 and 100% in 2010. Most manufacturers certified their 2007-2009 engines to a NOx limit of about 1.2 g/bhp·hr, based on a fleet average calculation.
l. Optional. Manufacturers may choose to certify engines to the California Optional Low NOx Standards of 0.10, 0.05 or 0.02 g/bhp·hr

The availability of these regulations means that some attention is being paid to the effects that these emissions have. In addition, it suggests that measures are being taken to reduce the amount that is being produced and released into the environment. This stands in contrast to the unregulated emissions which are discussed in the next section.

2.2 Unregulated Engine Emissions

It has been determined over the course of much research, that particulate number (PN) emissions from SI engines (premixed combustion) is of much less concern than those from CI engines (non-premixed combustion) [30]. There are three major mechanisms of PN emissions from SI engines: lead, organic particulates, and sulfates [31]. With the development of better fuels that only contain trace amounts of sulfur, and also make anti-knock

additives unnecessary, two-thirds of the mechanisms of SI PN emissions have been eliminated. Lastly, even though SI combustion occurs in a fuel rich environment, the conditions needed for PN emissions from an SI engine are usually as a result of malfunction, and not typical operation [30]. This mean that PN emissions from SI engines are comparatively minimal and shifts the focus onto CI engines due to the fact that particulate matter emissions are an intrinsic property of diffusion (non-premixed) combustion [32]. The PN emitted from CI engines is mainly a carbon-based material, soot, on which a medley of other organic materials has been absorbed. It is made of many tiny primary particles agglomerated into larger clusters which can have on average 4000 individual particles, and typical have a diameter of 15 to 30 nm [31].

Correlations between ambient particulate concentrations and adverse effects on the respiratory system, cardiovascular system have consistently been found. These include the comparative studies conducted by Hatch et al. [33] which showed that combustion particles have adverse effects on lung defensive health. Epidemiological studies by Brunekreef and Forsberg [34] have also shown that there is a negative relationship between particulate matter and human health.

Through research, it has also been determined that it is the finer particles that have the unfavorable effects on health. This is because the superfine particles, though potentially plentiful, do not contribute greatly to the mass of emissions. A wide variety of researchers have shown that nanoparticulate matter can have acute health effects on humans of any age [35–37]. Some researchers, Becerra et al. [38] have even discovered a relationship between autism and particulates. With this in mind, the importance of the study of particulate emissions cannot be understated. This is because reducing such emissions will also lead to a reduction in the associated adverse physiological effects.

It should be noted that PN is not completely unregulated. There have been some regulations in the EURO standards but these started with EURO 5b in 2013 and remained

unchanged at $6\times\ 10^{11}$ #/km with the introduction of EURO 6 in 2014. A progression on EURO regulations is shown below in Table 2.2.

Table 2.2: EURO regulations for passenger vehicles [39].

Stage	Date	CO	HC	HC+NOx	NOx	PM	PN
		g/km					*#/km*
Compression Ignition (Diesel)							
Euro 1†	1992.07	2.72 (3.16)	-	0.97 (1.13)	-	0.14 (0.18)	-
Euro 2, IDI	1996.01	1.0	-	0.7	-	0.08	-
Euro 2, DI	1996.01[a]	1.0	-	0.9	-	0.10	-
Euro 3	2000.01	0.64	-	0.56	0.50	0.05	-
Euro 4	2005.01	0.50	-	0.30	0.25	0.025	-
Euro 5a	2009.09[b]	0.50	-	0.23	0.18	0.005[f]	-
Euro 5b	2011.09[c]	0.50	-	0.23	0.18	0.005[f]	6.0×10^{11}
Euro 6	2014.09	0.50	-	0.17	0.08	0.005[f]	6.0×10^{11}
Positive Ignition (Gasoline)							
Euro 1†	1992.07	2.72 (3.16)	-	0.97 (1.13)	-	-	-
Euro 2	1996.01	2.2	-	0.5	-	-	-
Euro 3	2000.01	2.30	0.20	-	0.15	-	-
Euro 4	2005.01	1.0	0.10	-	0.08	-	-
Euro 5	2009.09[b]	1.0	0.10[d]	-	0.06	0.005[e,f]	-
Euro 6	2014.09	1.0	0.10[d]	-	0.06	0.005[e,f]	6.0×10^{11} [e,g]

* At the Euro 1..4 stages, passenger vehicles > 2,500 kg were type approved as Category N_1 vehicles
† Values in brackets are conformity of production (COP) limits
a. until 1999.09.30 (after that date DI engines must meet the IDI limits)
b. 2011.01 for all models
c. 2013.01 for all models
d. and NMHC = 0.068 g/km
e. applicable only to vehicles using DI engines
f. 0.0045 g/km using the PMP measurement procedure
g. 6.0×10^{12} 1/km within first three years from Euro 6 effective dates

This means that PN regulations are less than half a decade old which is infancy in the realm of standardized regulations. In addition, the limit has remained unchanged since its introduction. It is both of these factors that led to PN being labeled as unregulated.

This shows that there is need for a more fundamental understanding of PN which could easily be translated into better PN regulations. Note (from Table 2.2) that PM regulations have been around from the start of the EURO standards but PN regulations have only been around for five years.

2.3 Previous Work

While particle number (PN) regulations are new, there have already been studies on PN from various researchers over the last two decades.

In 1998, Kittelson published a study where the health effects of particulate matter (PM) were discussed [40]. It also outlined in great detail the structure and composition of the particles emitted from these engines and how they are formed. The thing to note here is that there already were proposed PN standards in 1998. These standards would limit the mass amount of the coarse and fine fractions separately as it was understood that going based solely on total PM could favor the production of massive amounts of potentially harmful particles with no check in place.

Kittelson published another paper in 2006 in which the possibility of a zero particulate emissions vehicle was discussed [41]. At the time, the use of diesel particulate filters (DPFs, with trapping efficiencies of $\geq$99%) was already a well known practice to reduce the particulate emissions from diesel engines, but Kittelson suggested the use of a continuously regenerating DPF (CR-DPF) with active catalysts to achieve even greater conversion efficiencies than standard DPFs. There had already been studies to determine which active agent was the most efficient at regenerating these filters. These cover a wide range, with perovskites (Ca-Ti oxide) [42–44], spinels [45, 46] and cerias (Cerium oxides) [47, 48]. There have even been studies into more exotic catalysts like ionically conducting ceramics like Yttria-Stabilized Zirconia (YSZ), with interesting results [49].

In 2015, Czerwinski et al. [50] found that there is a difference in PN emissions from gasoline engines depending on whether the engine is running cold or is running after it has been brought up to operating temperature. Their results show that there is a difference of up five times between cold and hot starts. They also found that there is a good repeatability of emissions levels when the engine is allowed to get up to operating temperature. Lastly, in concurrence with findings from the test cell (See Chapter 5), the most amount of particles is produced when the engine is run at a high speed/load combination.

Khalek et al. [51] found that there is a difference in both PN and PM based on the fuel that was used. Using a fairly new (at the time) vehicle, they found that the more volatile the

fuel was, the lower the total particle emissions were. They were able to confirm this using models to show that there was indeed a correlation between fuel boiling point (evaporative index) and the decrease in particles. The Khalek study was done on a gasoline direct injection (GDI) engine, but the results were again shown by De Filippo et al. [52] a year later, using a diesel engine and different diesel blends. De Filippo showed that the different fuels, ranging from ULSD to various bio-diesel blends, caused variations in the amount of PN produced. The paper highlighted that fact that the heating value of the fuel can also have a pronounced (even more so than combustion differences) effect on the amount of PN produced, suggesting that some adjustment of the engine is necessary to take full advantage of bio-diesel blends.

Another study showing the effects of fuel differences on PN is the 2012 study by Maricq et al. [53]. It showed that increasing the ethanol percentage to more than 30% causes a 30-45% reduction in the amount of PN produced even though particle size and distribution is unaffected. In addition to Khalek [51] and Maricq [53], Peckham et al. [54] have also studied turbocharged direct injection engines and found that instead of varying the fuel chemistry, PN can be reduced by simultaneously using direct injection and turbocharging. This was confirmed in the 2009 Myung study that found that GDI engines posses higher fuel efficiency and lower particulate emissions [55]. However Myung et al. [55] found that GDI engines produce excess particles at cold start, and during transient operation which has led to the use of parametric control strategies for mixture preparation, physical modification of the combustion chamber and the use of a DPF to mitigate the PN produced during these periods.

Further studies which investigated the relationship between PN and engine operating conditions have found that engine manufacturers have been able to successfully lower the amount of particulates by a great deal but in doing so have inadvertently raised the amount of nanoparticles present in the exhaust stream [56]. In addition, as suggested by Kittelson

in his 1998 study [40], nanoparticulate emissions may have to be regulated and there have been some regulations but Imad [51] has shown that there is still much to learn about PN as the same engine can both pass and fail different emissions tests by the same regulatory organization.

The studies presented here encompass only a small fraction of the amount of published work on PN and engines, so it is clear that a lot of time, energy and effort is already being dedicated to particulate emissions research. While that is true, almost all the studies focus on automotive engines and applications. This is because there are very stringent regulations on automotive emissions and manufacturers have to comply to stay competitive so there has been a push to study and reduce PN which is a positive benefit as the adverse health effects get mitigated.

2.4 Motivation

The work presented in this thesis is an evolution of work that has been done over the last few years in the Bucknell Powertrain Laboratory.

Historically speaking, smoke limits are reached by increasing the air-fuel ratio (AFR). The first study was to replicate that procedure to find out if there is any merit to it. The study looked into the effects of changing the air-fuel ratio on smoke and NO_x levels and was done on a 1.6L Peugeot four cylinder engine. It used the first iteration of the air injection system which is described later in Section 3.2.

The result of this study was that increasing AFR to high levels (> 200) caused a significant ($\sim$99%) reduction in smoke levels and slight ($\sim$10%) increase in NO_x. This is consistent with chemistry, as increasing the amount of air increases the available oxygen, which raises the oxidative chance resulting in a decrease in smoke particles. This also introduces more nitrogen which when combined with the combustion characteristics of a CI

engine raises the chance for the formation of various oxides of nitrogen.

From there, the next logical question was asked: As smoke is comprised of particulate matter, if smoke levels decrease, what happens to PN?

To do so, the ability to make particle number measurements was added to the test cell. This capability is further described in Section 3.3. In addition, the air injection system was refined and upgraded to be more reliably repeatable. The results of this study are shown in-depth in Chapter 5. In general, it was found that air injection reduced the PN concentration, however, once normalized using the engine power output, it was found that there was very little change in PN concentrations. This was counterintuitive to what was expected as a reduction in smoke was thought to correlate with a reduction in PN. This led to the next question: Would operating condition have an effect on PN?

This question, along with the other outlined in the thesis objectives, is what the work described in this thesis is trying to answer.

The current work focuses on an air-cooled industrial diesel engine, popularly used in industrial and agricultural applications, and also for backup power. Smaller engines such as these are the most common source of backup power throughout the world because of their increased portability relative to larger engines. Since these engines generally run at fixed operating points, and since the same power might be obtained from different combinations of speed, load, injection timing, and other operating parameters, it might be possible to reduce PN emissions based solely on choice of engine operating condition.

Despite the ubiquity of these engines in industrial and agricultural applications, all of the studies presented thus far have focused on automotive engines because of existing or impending PN emission limits. There are a few studies that have attempted to characterize and measure the PN from non-automotive engines. One of these is the work done by Alander et al. [57] which characterized the effects of fuel formulation and after-treatment of the particulate emissions from a two stroke chainsaw engine. A similar study was done

by Christensen et al. [58] but for a four stroke lawn mower engine and they found that the addition of an oxidizing after-treatment reduced particulate emissions. However, both of these studies focused on after-treatment as opposed to raw emissions from the engine itself.

Since there is little published literature, this proposed work is similar to that of breaking a new frontier as similarly sized, air-cooled, four stroke engines have not been comprehensively studied. As such, the work has been kept very broad to avoid over-specificity and to see if general characterization of PN from such engines can be performed. This will be done by addressing some general questions: how much PN is actually produced by these engines? And, how are these production levels affected by operating conditions?

Chapter 3

TESTING APPARATUS

This chapter will discuss the design of the test cell including both the addition of new equipment, and the modification of existing equipment and infrastructure to allow proper testing.

3.1 Engine Setup Overview

The test cell is the result of a collaborative effort between students, faculty and support staff. It was designed and built using design criteria established by the needs of previous researchers. The most critical criterion was determined to be safe and user friendly operation. This is reflected in the fact that any and all parts that could pose any danger to the operator have been appropriately guarded and shielded to prevent potential harm.

A single cylinder, mechanically injected, air-cooled industrial Yanmar diesel engine (max output 8.6 HP) is the engine that will be used for this work. Table A.1 in Appendix A lists the specifications for this engine. A picture of the engine is shown below in Figure 3.1.

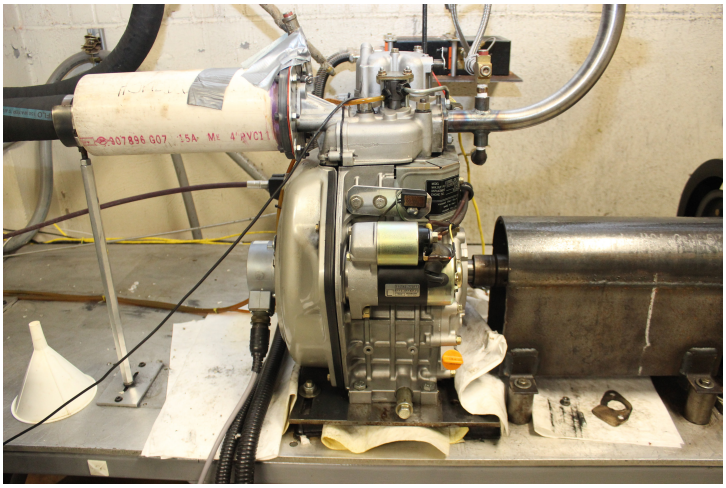

Figure 3.1: Single cylinder diesel engine.

The engine is rigidly coupled to a motor generator that serves as the system dynamometer. This particular dynamometer is capable of absorbing 20 HP at a maximum speed of 1800 RPM. As the rated engine speed is 3600 RPM, a 2:1 pulley reduction system was used to get the engine speed into the right range so as not to damage the dynamometer. Given the specifications of the dynamometer, a quick calculation shows that it is capable of absorbing a maximum torque of around 58 lb-ft ($\sim$79 Nm) of torque which is more than enough for this application. A picture of the motor-generator dynamometer is shown below in Figure 3.2, and as coupled to the engine in Figure 3.3.

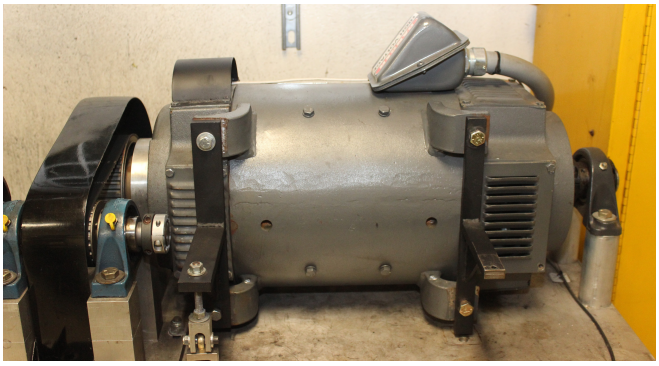

Figure 3.2: Motor-generator repurposed as a dynamometer.

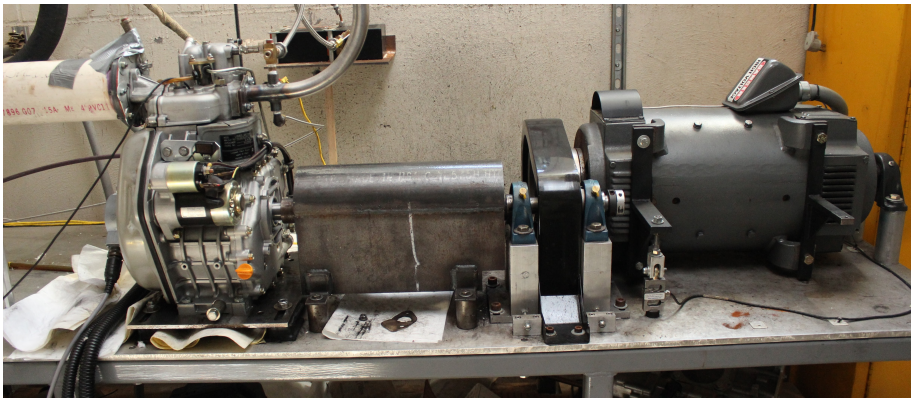

Figure 3.3: Dynamometer coupled to the engine.

The dynamometer is supported on its rotational axis which leaves the casing free to rotate. This allows the measurement of the torque by using a load cell. The rotation of the dynamometer shaft induces a reactionary rotation on the case that is counteracted by the load cell which when combined with the geometry of its mounting location can be used to obtain the torque produced by the engine. A picture of this setup is shown below in Figure 3.4.

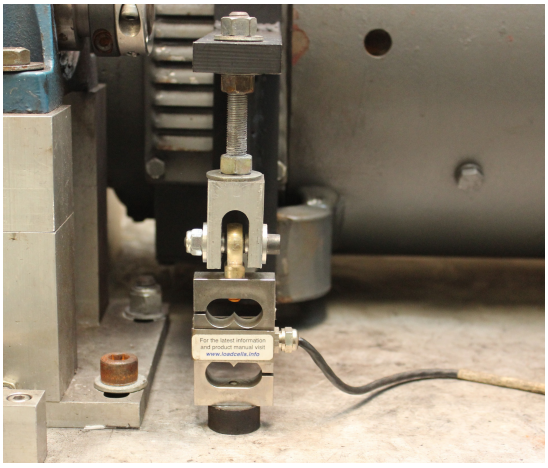

Figure 3.4: Torque measuring load cell setup.

In addition to the torque, speed measurement is also important. To achieve this, a Hall effect trigger sensor was employed. It is mounted within the enclosure of the dynamometer and used to sense when each of the blades on the motor cooling fan passes its mounting

location. Each time a blade passes, it causes the sensor to trigger and a pulse is created. An electronic counting system turns the amount of pulses into speed in RPM. The mounting of the sensor is shown below in Figure 3.5.

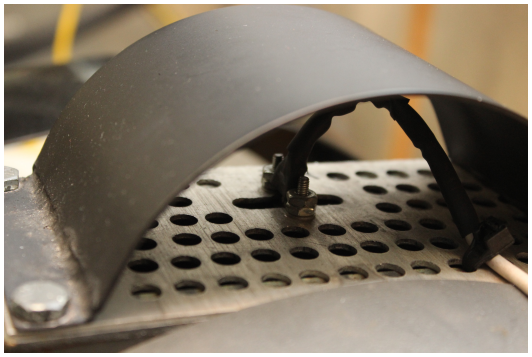

Figure 3.5: Hall effect trigger sensor mounting.

The power generated by the dynamometer has to be dissipated in some manner. In this case, it is used to drive a bank of resistance heaters submerged in a tank that is continually cooled by city water. A picture of the tank is shown below in Figure 3.6. Note the high voltage resistor box on the side.

Figure 3.6: Resistor bank cooling setup.

The engine is controlled from a student designed box that is shown below in Figure 3.7.

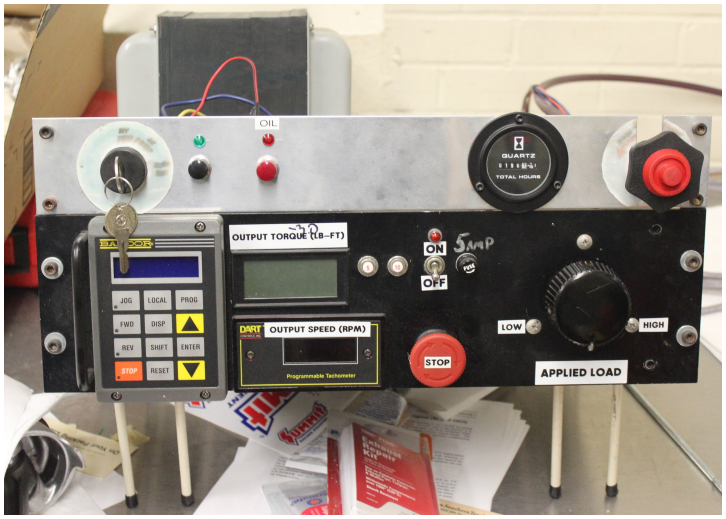

Figure 3.7: Student built engine control box.

First and foremost, the box contains the power switch for the engine systems and also the starter switch. It also contains all the physical controls for the engine. The black dial on the right controls a transformer that varies the current supplied to the dyno which varies the resistive torque to the engine. The red knob above that is a push-pull cable that is connected directly to the throttle on the engine which is used to vary the engine speed. The readouts in the middle are for the current engine speed and torque and display the results of the student-built electronic systems to output easily viewable data. There is a stop button to cut all power to the fuel pump and dyno in the case of an emergency.

The test cell is also capable of measuring the in-cylinder pressure during combustion. This is achieved by a pair of sensors. One of these sensors is a BEI HS35 encoder that is capable of 360 pulses per rotation (ppr) which equates to one pulse for every crank angle the engine rotates through. These pulses are used to trigger the second sensor which is a piezoelectric pressure transducer that is attached to the cylinder head. The encoder is shown below in Figure 3.8.

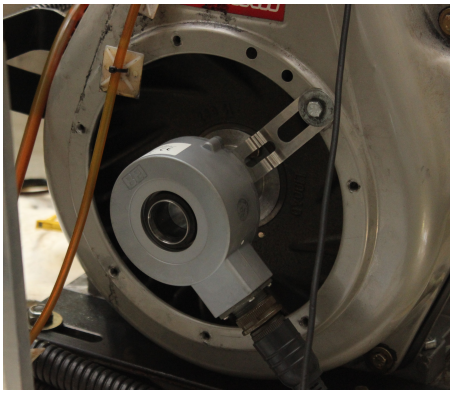

Figure 3.8: Encoder as mounted on the engine.

3.2 Air Injection System

The engine is fed by fresh air that goes through a plumbing network that is designed to work with the air injection system. The intake air goes through a laminar flow element (LFE) which is setup to measure the intake side pressure, and the differential pressure. A picture of the LFE is shown below in Figure 3.9.

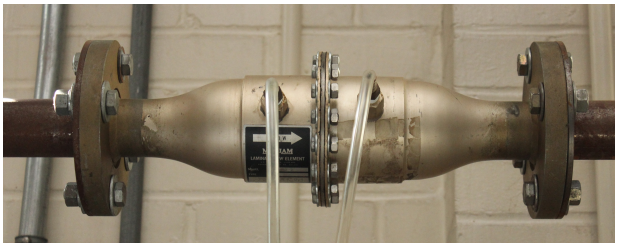

Figure 3.9: Laminar flow element.

To explore higher air-fuel ratios than natural aspiration can provide, forced induction was employed. The air injection system is a culmination of prior summer work and a senior design project. The source of external air is a compressor and drier outside the laboratory, designed to supply shop air to the entire college of engineering.

The shop air comes into an surge accumulator that is used to reduce the effects of system pressure fluctuations when other machinery that require shop air are switched from on to off and vice versa. Due to the fact that the test cell is in the basement, the shop air

has a higher water vapor content. This can cause corrosion problems most noticeably in the accumulator so multiple steps were taken to ensure that the air going into the tank was as dry as possible. This involved two water traps, one at the lab line inlet and one at the accumulator inlet, a manual drain valve on the inlet which is vented periodically during testing, and an automatic valve on the bottom of the tank that vents every 45 mins.

The air from the tank is then sent into the intake line, first through a pneumatic three-way valve with an actuation pressure of $\sim$ 80 psi (fed off a regulator at the top of the accumulator), then a pressure regulator to ensure a steady state volumetric flow rate during injection events and then the LFE as described above. Both of these are shown below in Figure 3.10.

Figure 3.10: Regulator (bottom), and pneumatic three-way valve (top, blue).

From prior testing, it was observed that the pressure regulator resulted in a steady flow rate, but the actual pressure in the intake system was slightly less than the set pressure. During preliminary work for this research study, different regular pressure set-points were investigated (0 psi, 5 psi, 10 psi, 20 psi and 30 psi). It was found that 30 psi resulted in very high cylinder pressure (about 3000 psi), while the set-points below 20 psi produced negligible amounts of boost. 20 psi was therefore chosen as a constant regulator setting for

all operating conditions as it provided the best compromise between cylinder pressure and boost (∼18 psi), and served the purpose of producing a wide range of air-fuel ratios from 30, all the way up to 200.

An overview of the air injection system is shown below in Figure 3.11 and 3.12.

Figure 3.11: Overview of the accumulator.

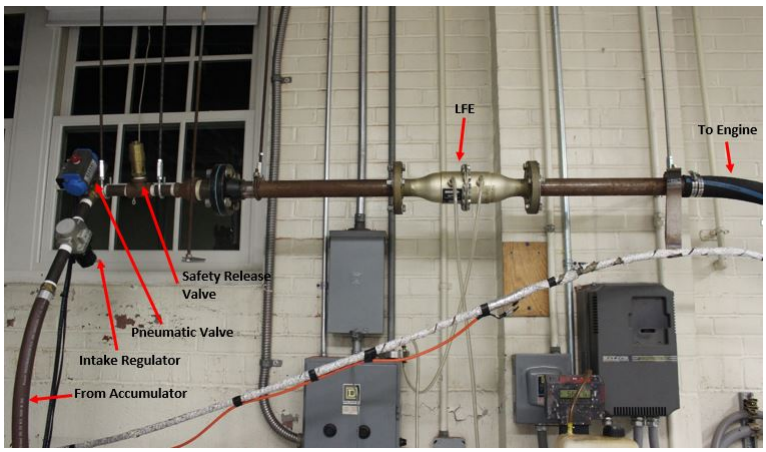

Figure 3.12: Overview of the intake line.

3.3 Emissions Measurements

Since one of the main focuses of this thesis was to study emissions, the test cell has to be capable of making emissions measurements.

The exhaust pressure is measured about 3" from the exit of the cylinder using a 5 psi OMEGA PX309 series pressure transducer. This location was chosen because the exhaust pressure reduces along the exhaust tubing until it gets to atmospheric pressure when it reaches the end. This negates the need for a differential sensor as the exhaust flow rate can be calculated using the measured exhaust pressure and atmospheric pressure. As the pressure was being measured so close to the cylinder, the temperatures were beyond the operating range for the sensor. To combat this, natural convection calculations were used to determine the required length of stainless steel tubing to reduce the temperature to a low enough level to not damage the sensor.

The emissions test bed is fed using a line that is connected to a port on the exhaust tubing, close to the engine cylinder exit. This line is heated to 300^{o}C to ensure that all volatile particles in the sample evaporate before reaching the analyzers. The sample is then sent through a heated filter to reduce the temperature to 160^{o}C before entering the chiller where water vapor is condensed out to ensure dryness. The Figures below show the setup described above.

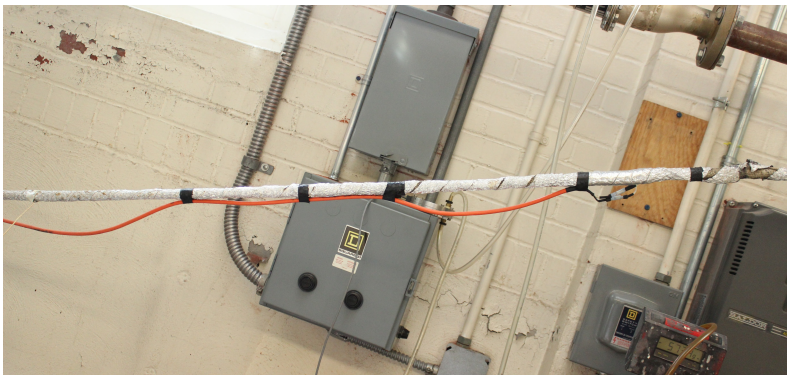

Figure 3.13: Heated sample line.

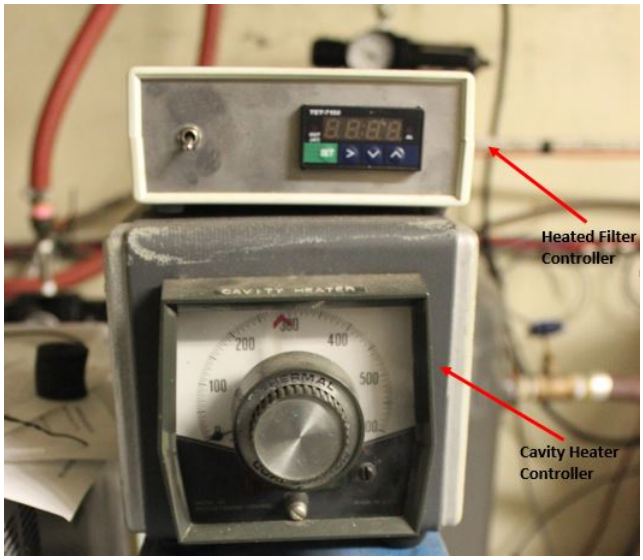

Figure 3.14: Heated sample line and cavity heater controller.

Figure 3.15: Heated filter and chiller.

One of the major pieces of emissions equipment is the CAI Systems 600 Series Heated Flame Ionization Detector (HFID). The HFID is used to measure total hydrocarbon (THC) concentration in the exhaust stream. It has an oven that is heated to 191^{o}C using an air and 40/60 Hydrogen-Helium flame, and which contains two electrodes to create an electrostatic field. When the sample enters the oven, it is ionized by the flame and the ionic separation in the electrostatic field causes a small current which is proportional to the amount of hy-

drocarbons in the sample. The HFID is shown below in Figure 3.16.

Figure 3.16: CAI 600 Series heated flame ionization detector.

The second of these pieces of equipment is the Horiba Instruments PG-250 Portable Gas Analyzer. It is a multi-gas analyzer capable of measuring CO, CO_2, SO_x, NO_x and O_2. It uses a pneumatic non-dispersive infrared (NDIR) sensor to measure CO and SO_x, a pyro-NDIR for CO_2, cross-flow modulation for NO_x and a galvanic cell for O_2. The Horiba is shown below in Figure 3.17.

Figure 3.17: Horiba Instruments PG-250 portable gas analyzer.

Particle measurement is taken care of by a TSI 3090 Engine Exhaust Particle Sizer

(EEPS) (Figure 3.20) which is a spectrometer that operates on the electrical mobility principle. The exhaust is collected by a TSI 397020A Rotating Disk Thermodiluter (Figure 3.18) wherein a rotating disk with 8 semi-hemispherical cavities mixes exhaust and fresh air by the alternate scooping of each gas stream. The sample is further diluted in a TSI 397030 thermal conditioner (Figure 3.19) prior to entering the particle sizer. Both primary and secondary dilution steps are set to occur at high temperatures (180 ^{o}C and 300 ^{o}C respectively) to prevent the formation of volatile and semi-volatile nanoparticles. The overall dilution ratio was 167.

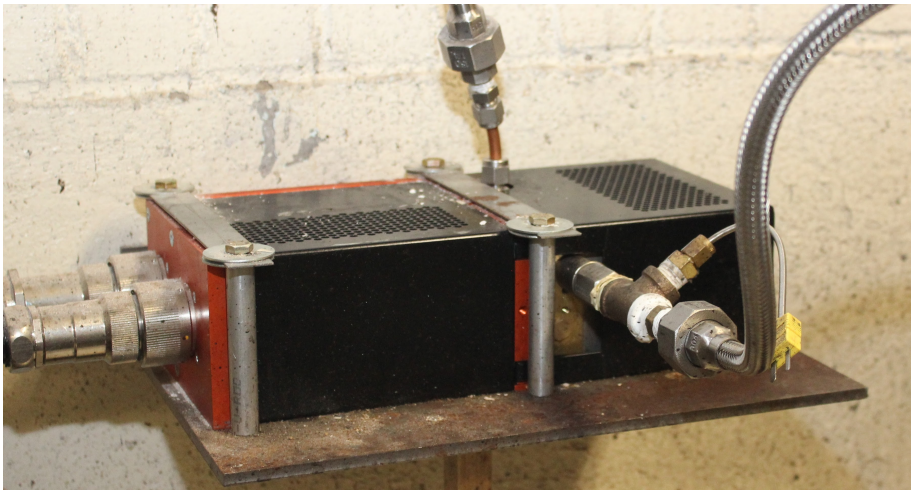

Figure 3.18: TSI 3907020A rotating disk thermodiluter.

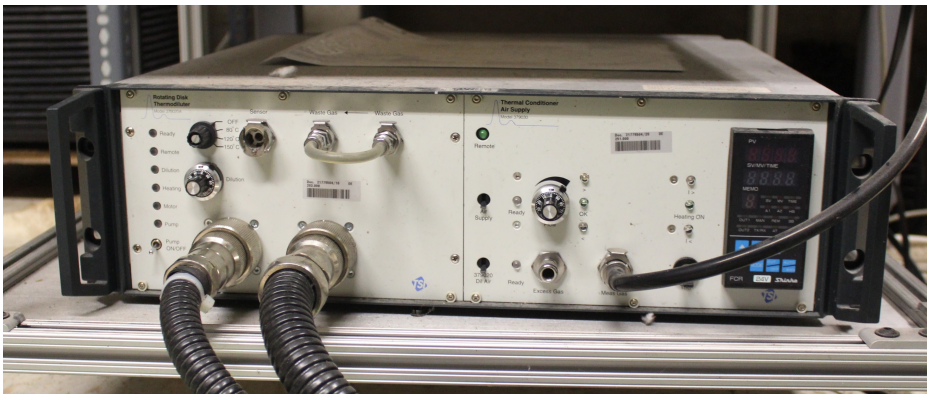

Figure 3.19: TSI 397030 thermal conditioner.

Figure 3.20: TSI Model 3090 engine exhaust particle sizer.

Chapter 4

TESTING METHODOLOGY

This section will discuss the testing plan and overall analysis.

4.1 Testing Plan

The purpose of the research experiment was to run an engine at various operating points and to determine whether these operating points affect the amount and quality of PN that the engine emits.

Seventy-five operating conditions corresponding to five loads at each of the three engine speeds at five fuel injection timings were explored for the study: 0% (0ft-lb), 25% (3 ft-lb), 50% (6 ft-lb), 75% (9 ft-lb) and 100% (12 ft-lb) load at 2000 RPM, 2500 RPM and 3000 RPM at 15^{o}, 15.5^{o}, 16^{o}, 16.5^{o}, and 17^{o} all degrees before top dead center (BTDC). Ten more operating conditions, for a total of 85, at 2000 RPM, and all load levels were tested at 4^{o}, 10^{o} (also BTDC) to further explore the effects of extreme retardation.

The operating speeds were chosen to encompass the useful portions of the torque curve, excluding high (>3000 RPM, fuel consumption rises sharply) and low (<2000 RPM, excessive vibration) speed operation. The behavior of the engine was well-understood from

a previous biofuel study on it [59], in the Bucknell Powertrain Laboratory. Each operating condition was stabilized for 10 minutes before any data was acquired. PN, temperature and pressure data were acquired and averaged over a subsequent 5 minute collection period.

The testing plan was essentially the same for the forced induction tests except for the fact that air was injected into the engine by switching the pneumatic 3-way valve (Figure 3.10) and the engine was allowed to stabilize over an additional five minute period. Data acquisition was then repeated over the next five minute period in the same manner as for naturally aspirated operation.

One thing of note is that emissions data was not collected for the forced induction test. This is due to the fact that the emissions equipment setup requires a fairly long time to reach steady state, on the order of 10 minutes for natural aspiration. The stabilization time is even longer for forced induction which when coupled with the large amount of operating points made collecting emissions data infeasible for forced induction. In addition, when an operating point was allowed to fully stabilize (after about 25 minutes for 6ft-lb at 2500 RPM and 17^{o} BTDC), many of the readings were underrange which suggests that even if the data was collected, it would not be analyzable or contribute to the results and no conclusions could be drawn from it.

4.2 Analysis

The analyses of the collected data are outlined below. The data collected from the engine was used to achieve a clearer understanding of the combustion characteristics of the engine. Once that was done, these combustion characteristics can be correlated to PN levels. There were two major results required: the heat release rate profile (combustion) and the specific PN output (emission) of the engine.

4.2.1 *Heat Release Rate*

The first step was the refinement of the raw in-cylinder pressure data. The ability to collect this data was a feature that was added to the Test Cell in the summer of 2015. The raw data is 36000 individual points for each of the eighty-five operating conditions.

The raw data was divided into fifty units, each one 720 points long (for each 4-stroke engine cycle), which were then averaged to produce a single pressure trace for each operating point. This is possible as the engine crank angles and pressures are synced through the encoder making the timing constant between cycles. Averaging multiple cycles is necessary to reduce the effects of cycle-to-cycle variations in the pressure measurements due to changes in combustion. This makes the end result more representative of that particular operating condition.

Once this pressure trace was obtained, it was pegged. Pegging is the process of using a reference pressure level to counteract the offset drift of a piezoelectric pressure sensor due to thermal sensitivity. The in-cylinder pressure data in this study was pegged to the intake manifold pressure. This was done by setting the minimum value of the trace to the recorded pressure of the intake manifold. It should be noted that pegging is done to absolute pressure so the pressure trace was first converted from gage pressure by adding one standard atmosphere (101.325 kPa) to it.

The compression ratio of an engine is defined as the ratio of the maximum cylinder volume to the minimum cylinder volume and is given as:

$$r_{\mathrm{c}} = \frac{\textit{maximum cylinder volume}}{\textit{minimum cylinder volume}} = \frac{V_{\mathrm{d}} + V_{\mathrm{c}}}{V_{\mathrm{c}}} \tag{4.1}$$

Where r_{c} is the compression ratio, V_{d} is the displaced volume swept by the piston, and V_{c} is the clearance volume.

Rearranging Equation 4.1 makes it possible to solve for the clearance volume, given

as:

$$V_{\mathrm{c}} = \frac{V_{\mathrm{d}}}{r_{\mathrm{c}} - 1} \tag{4.2}$$

The displaced volume as a function of crank angle was obtained using the geometric relations [60], and is given as:

$$V_{\mathrm{d}}(\theta) = \frac{\pi B^2}{4}(l + a + s(\theta)) \tag{4.3}$$

Where B is the bore of the cylinder, l is the length of the connecting rod, a is the crank radius, also defined as half the stroke, θ is the crank angle in degrees, and $s(\theta)$ is a function of crank angle that defines the distance between the piston pin axis and the crank axis. The definition of $s(\theta)$ is given as:

$$s(\theta) = acos(\theta) + (l^2 - a^2 sin^2(\theta))^{\frac{1}{2}} \tag{4.4}$$

Putting Equation 4.2, Equation 4.3 and Equation 4.4 together, it is possible to come up with an expression for the total volume of the cylinder given as:

$$V_{\mathrm{tot}}(\theta) = \frac{V_{\mathrm{d}}}{r_{\mathrm{c}} - 1} + \frac{\pi B^2}{4}(l + a(1 - cos(\theta)) - (l^2 - a^2 sin^2(\theta))) \tag{4.5}$$

The easiest method to find TDC is to obtain the motoring curve for the engine. The motoring curve is an in-cylinder pressure trace collected when the engine is cranked through a complete cycle without combustion taking place; usually achieved using an external motor, such as the engine starter motor. From knowledge of piston-cylinder devices, the point of maximum pressure occurs at the point of minimum volume. As TDC is the point in the cycle of minimum volume, this means that by extension, TDC occurs at the point of maximum pressure.

This method is correct in its application of the relationship between volume and pressure in a closed system of fixed mass. However, it falls short because it does not take thermodynamic effects into consideration. This is because by its very nature, obtaining the motoring curve means that combustion is ignored. This means that there is going to be some lag between the point of maximum pressure and TDC. Tazerout et al. have shown that there is indeed a negative phase difference between the point of maximum pressure and TDC due to thermodynamics [61]. In addition, crevice effects and blow-by can contribute to this phase difference.

Many methods have been created to accurately determine TDC because of this phase difference. The previously mentioned work of Tazerout et al. used an entropy based method in which the location of TDC was determined by looking at the symmetry of the motoring curve with respect to the peak cylinder temperatures [61]. This turns out to be a very accurate method and a common thread is that a lot of the more accurate TDC-determination methodologies are based on thermodynamics and require complex calculations. This is not a bad thing as these methods are quite accurate, but if a simpler method is possible with comparable accuracy, then that would be a better option.

An interesting study was done by Nilsson and Eriksson in which they compared five methods of TDC determination. These methods covered a wide range, from the simple, setting the TDC to the point of maximum pressure, to the more involved, comparing polytropic correlation to inflection points in the pressure trace. What they found is that on average, the distance error in the location of TDC was between -0.00041^{o} and -0.80^{o}.

It should be of no surprise that the method with the greatest error is the simplest method as outlined at the start of this step. This is not good because Piptone and Beccari discovered that a 1^{o} shift in TDC location can cause up to a 25% error in heat release calculations [62]. However, because the average value of the distance lag is known, it is still possible to use the first method. After the motoring curve is obtained and the point of

maximum pressure is determined, a correction is applied by setting the location of TDC to 0.80^{o} ahead of that point. This method was verified using by using a dial gauge and it was found that the error was less than a 0.001in which translates to less than 0.1^{o}.

As the LFE was calibrated to produce a maximum pressure differential of 8 inH_2O at a flow rate of 100 CFM, it was a simple matter of multiplying the measured pressure differential across the LFE by this calibration factor. The volumetric flow rate of air into the engine is given as:

$$\dot{V}_{\text{air}} = \Delta P_{\text{LFE}} \times k_{\text{LFE}} \tag{4.6}$$

Where $\dot{V}_{\text{air}}$ is the volumetric flow rate of air into the cylinder, ΔP_{LFE} is the pressure differential across the LFE, and k_{LFE} is the LFE calibration value.

The intake mass flow rate is the intake volumetric flow rate multiplied by the density of the intake air, determined using the ideal gas law and are given as:

$$\dot{m}_{\text{air}} = \dot{V}_{\text{air}} \times \rho_{\text{air}} \tag{4.7}$$

$$\rho_{\text{air}} = \frac{P_{\text{int}}}{R_{\text{specific}} T_{\text{int}}} \tag{4.8}$$

Where $\dot{m}_{\text{air}}$ is the mass flow rate of the intake air, ρ_{air} is the density of the intake air, P_{int} is the pressure in the intake manifold, R_{specific} is the specific gas constant of air, and T_{int} is the temperature of the intake manifold.

Ignoring any leaks through the piston rings, the total mass flow through the engine is equal to the sum of the mass of the air trapped in the cylinder when the valves close, and the mass of the fuel injected. The total mass of air and fuel in the cylinder is given as:

$$\dot{m}_{\text{tot}} = \dot{m}_{\text{air}} + \dot{m}_{\text{fuel}} \tag{4.9}$$

It should be noted that $\dot{m}_{\text{fuel}}$ is a quantity obtained by mass of fuel consumed by the

engine over a specific time period, which was two minutes in the case of this study.

Syncing the volume and pressure data is an important step as it allows the use of the ideal gas law to calculate the cylinder temperatures. This would otherwise be impossible as the resultant temperatures would be grossly incorrect due to the wrong values of volume and pressure being matched up in the equation. This temperature determination is given as:

$$T_{\text{cyl}} = \frac{P_{\text{cyl}} V_{\text{tot}}}{m_{\text{tot}} R_{\text{specific}}} \tag{4.10}$$

Where T_{cyl} is the cylinder temperature, P_{cyl} is the cylinder pressure, and R_{specific} is the specific gas constant of the working fluid, which in this case was chosen as air. It should be noted that this was done because the ratio of the mass of fuel to the mass of air is negligible.

The ratio of specific heats is the ratio of the specific heat at constant pressure and the specific heat at constant volume. The determination of γ is given as:

$$\gamma = \frac{c_{\text{p}}}{c_{\text{v}}} \tag{4.11}$$

Where γ is the ratio of specific heats, c_{p} is the specific heat at constant pressure, and c_{v} is the specific heat at constant volume.

The specific heat requires a non-negligible amount of work to determine from first principles, which when combined with the fact that there are 36000×85 points, and two specific heats means a lot of computation. To simplify the calculation, the definition of the specific gas constant was employed:

$$R_{\text{specific}} = c_{\text{p}} - c_{\text{v}} \tag{4.12}$$

Rearranging Equation 4.12, it is possible to make c_{v} the subject of the equation. The

result of this is given as:

$$c_{\mathrm{v}} = R_{\mathrm{specific}} - c_{\mathrm{p}} \tag{4.13}$$

With a relation for c_{v}, it can now be substituted back into Equation 4.11. This new relationship is given as:

$$\gamma = \frac{c_{\mathrm{p}}}{c_{\mathrm{p}} - R_{\mathrm{specific}}} \tag{4.14}$$

This simplifies the calculation as only the specific heat at constant pressure has to be calculated. As the temperature was previously calculated in the analysis process, an empirical model relation was used to calculate c_{p}, as another practical method of simplification. The model used below is of cubic order and is dependent on the temperature of the cylinder. This makes the use of the model possible as the cylinder temperature has already been determined from the collected data. The model is given as:

$$\begin{aligned} \overline{C}_{\mathrm{p}} &= a + bT_{\mathrm{cyl}} + cT_{\mathrm{cyl}}{}^2 + dT_{\mathrm{cyl}}{}^3 \\ a &= 28.11 \\ b &= 0.1967 \times 10^{-2} \\ c &= 0.4802 \times 10^{-5} \\ d &= -1.966 \times 10^{-9} \end{aligned} \tag{4.15}$$

Where a, b, c and d are the empirical model fit coefficients, and T_{cyl} is the cylinder temperature. This model was also chosen due to its low intrinsic errors, with a maximum of 0.72% and an average value of 0.33%. However, due to the fact that this is an empirical model, the temperature has to be limited between a minimum of 273K and a maximum of 1800K.

With the above calculations done, it was then possible to calculate the heat releases. There are two heat release values calculable. The first of these is the net heat release rate.

This represents the amount of heat added to the combustion chamber as a function of the progression of the combustion process. It is usually represented in energy units per degree and is given as:

$$\frac{d\dot{Q}}{d\theta} = \frac{\gamma}{\gamma-1}PdV - \frac{1}{\gamma-1}VdP \tag{4.16}$$

Where $\frac{d\dot{Q}}{d\theta}$ is the net heat release rate, and dV and dP are the first derivative of the cylinder volume, and cylinder pressure respectively.

The second is the cumulative heat released which represents the total amount of heat added to the combustion chamber over the entire combustion process. This is usually represented in units of energy. The determination of the cumulative heat release is trivial because it is simply the integral of the net heat release.

4.2.2 *Energy Specific Particle Number & PN Production Rate*

The first step was to calculate the exhaust density. This was done using the Ideal Gas Law, with the exhaust pressure and exhaust temperature as the inputs. This is given as:

$$\rho_{\text{exh}} = \frac{P_{\text{exh}}}{RT_{\text{exh}}} \tag{4.17}$$

Where ρ_{exh} is the exhaust density, P_{exh} is the pressure in the exhaust manifold, R is the universal gas constant, T_{exh} is the temperature of the exhaust stream.

Using the Law of Conservation of Mass, the mass flow rate of the exhaust stream is equal to the mass flow rate of the intake stream. This means that the exhaust volumetric flow rate is the total mass flow rate from Equation 4.9 divided by the exhaust density calculated in Equation 4.17. This is given as:

$$\dot{V}_{\text{exh}} = \frac{\dot{m}_{\text{tot}}}{\rho_{\text{exh}}} \times 1e6 \tag{4.18}$$

Where $\dot{V}_{\text{exh}}$ is the volumetric flow rate of the exhaust stream. Multiplying by the conversion factor above converts the volume basis from m^3 to cm^3. This is necessary as the EEPS records its concentrations in the latter basis.

The determination of the power produced by the engine was done by multiplying the torque and speed of the engine, and then applying the proper conversion factor to obtain a result in kW. This relationship is given as:

$$P_{\text{eng}} = T_{\text{eng}} \times \omega_{\text{eng}} \times \frac{1.36}{9.55} \tag{4.19}$$

Where P_{eng} is the power produced by the engine, T_{eng} is the torque produced by the engine, ω_{eng} is the speed of the engine.

The PN production rate was obtained by multiplying the PN concentration with the exhaust volumetric flow obtained from Equation 4.18. The PN production rate is given as:

$$\dot{R}_{\text{PN}} = C_{\text{PN}} \times \dot{V}_{\text{exh}} \times 3600 \tag{4.20}$$

Where $\dot{R}_{\text{PN}}$ is the PN rate of production of the engine and C_{PN} is the PN concentration in the exhaust stream. Multiplying by the conversion factor above converts the time basis from seconds to hours. This was necessary to obtain a result in the required unit of energy.

With the above calculations done, it was then possible to calculate the energy specific PN. This was done by dividing the PN production rate by the power. This is given as:

$$R_{\text{PN,specific}} = \frac{\dot{R}_{\text{PN}}}{P_{\text{eng}}} \tag{4.21}$$

Where $R_{\text{PN,specific}}$ is the energy specific PN.

Chapter 5

RESULTS & DISCUSSION

This chapter details the results that were obtained using the testing procedures and analyses outlined in the previous chapter. In addition, a discussion will be presented, using these results as the basis for any claims made.

5.1 Combustion Results

This section will present the data collected during engine combustion using the analysis methodology outlined in Section 4.2.

Volume

The cylinder volume as a function of crank angle is shown below in Figure 5.1.

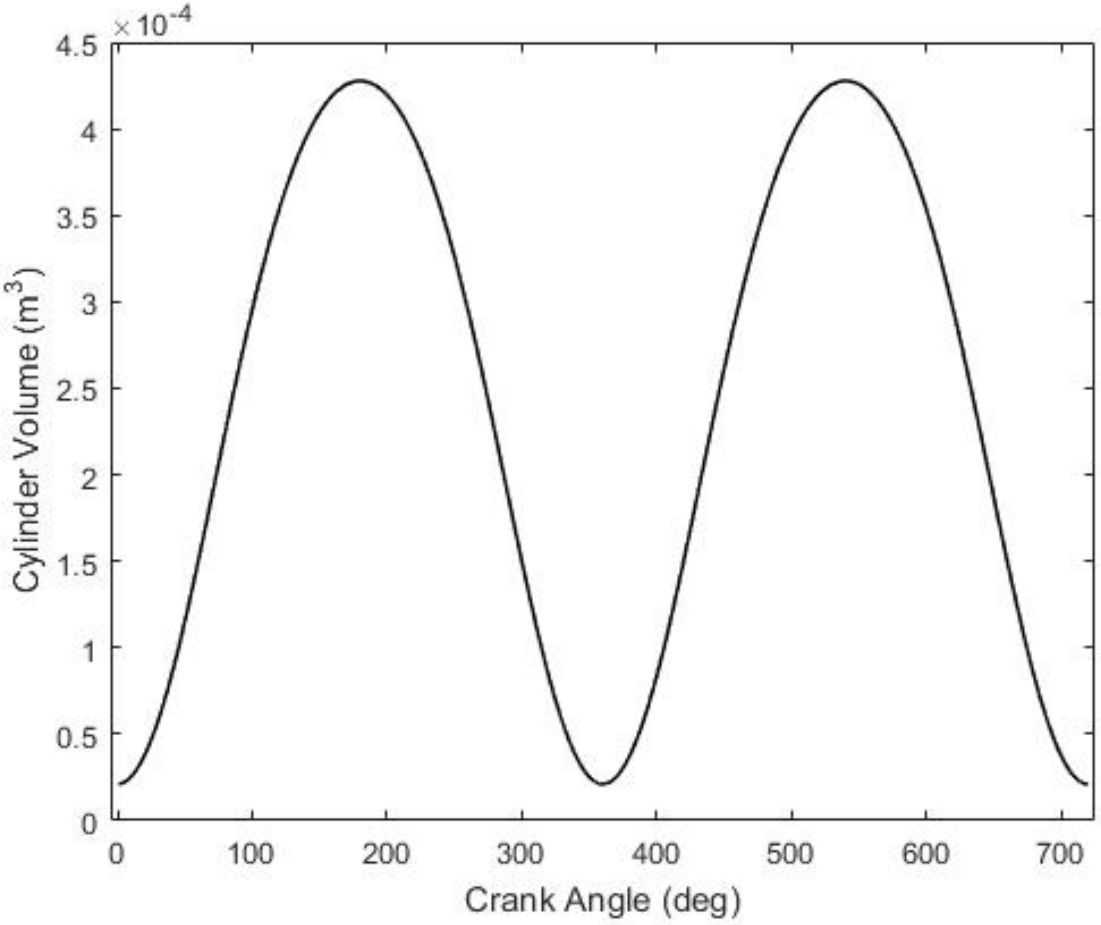

Figure 5.1: Cylinder volume as a function of crank angle.

As the cylinder volume is solely dependent on the position of the piston within the cylinder (crank angle), it is constant and doesn't vary as the operating points are changed.

In-Cylinder Pressure

Figures 5.2 and 5.3 show the variation of cylinder pressure vs. crank angle with torque at 2500RPM and 16^{o} BTDC.

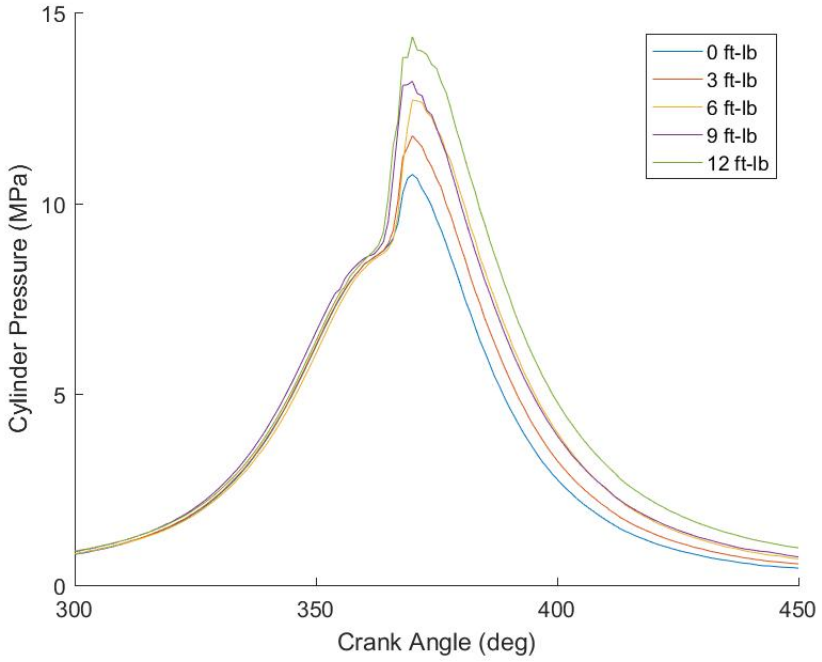

Figure 5.2: Cylinder pressures at 2500RPM and 16 ^{o}BTDC (natural aspiration).

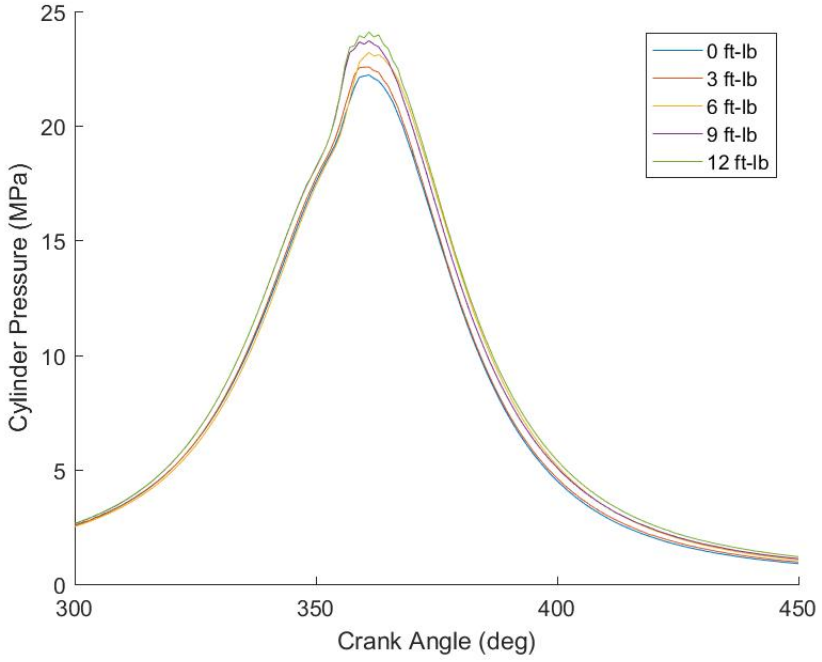

Figure 5.3: Cylinder pressures at 2500RPM and 16 ^{o}BTDC (forced induction).

Cylinder pressure is directly related to the indicated mean effective pressure (IMEP),

which in turn is directly related to torque. This means that as the load is increased, it would be expected that the cylinder pressure would increase as well which is confirmed by Figures 5.2 and 5.3. This is a trend that is observed at all speed and timing combinations regardless of air injection scheme.

Figure 5.4 shows a comparison between cylinder pressures for natural aspiration and forced induction.

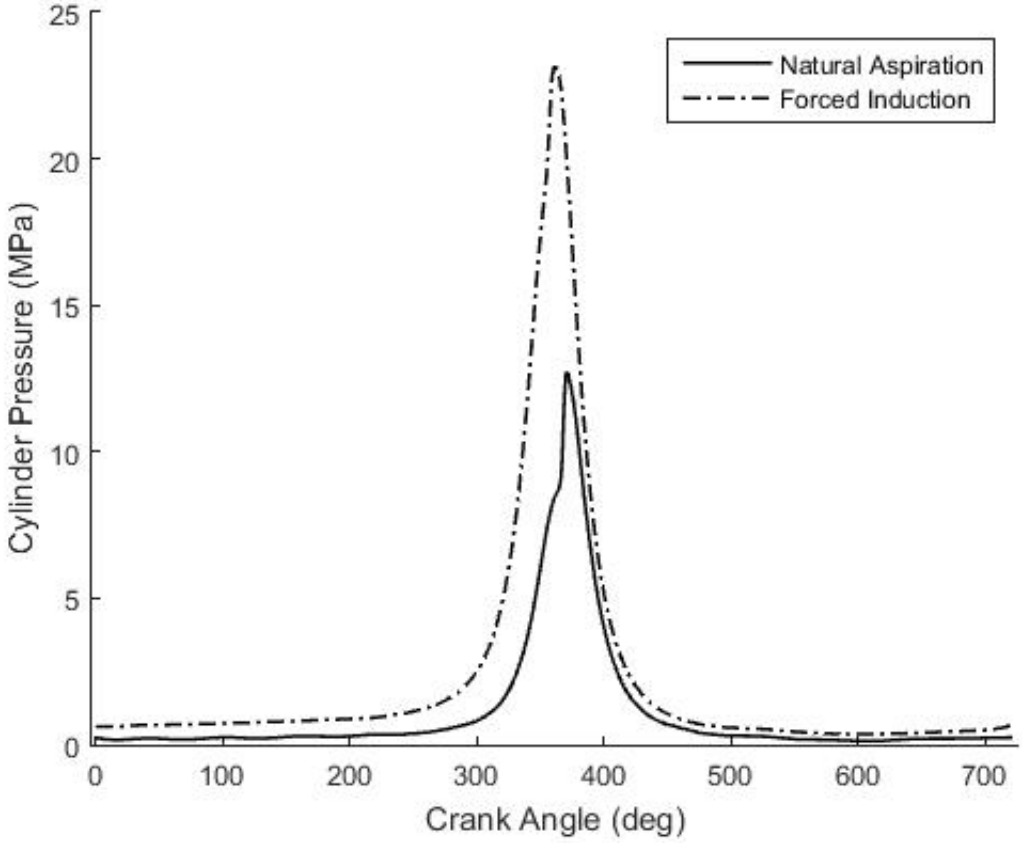

Figure 5.4: Comparison of cylinder pressure between natural aspiration and forced induction at 2500RPM, 6 ft-lb and 16 ^{o}BTDC.

It can be seen that the forced induction curve reaches a higher maximum pressure than the one for natural aspiration. This is because the cylinder is charged to a higher pressure prior to combustion. Another thing to note is that the curve for forced induction sits slightly higher. This is due to the fact that the pressure trace is pegged to the manifold

pressure which is greater when air is being forcibly inducted to the engine.

Also shown in Figure 5.4 is that there is a lot less premixing during forced induction. Visually, this can be concluded by observing the much smaller premix drop-off (kink) in pressure also seen when Figures 5.2 and 5.3 are compared. It is also evidenced by the fact that the minimum value of the derivative of cylinder pressure is higher for forced induction than it is for natural aspiration. This is confirmed in Figure 5.5.

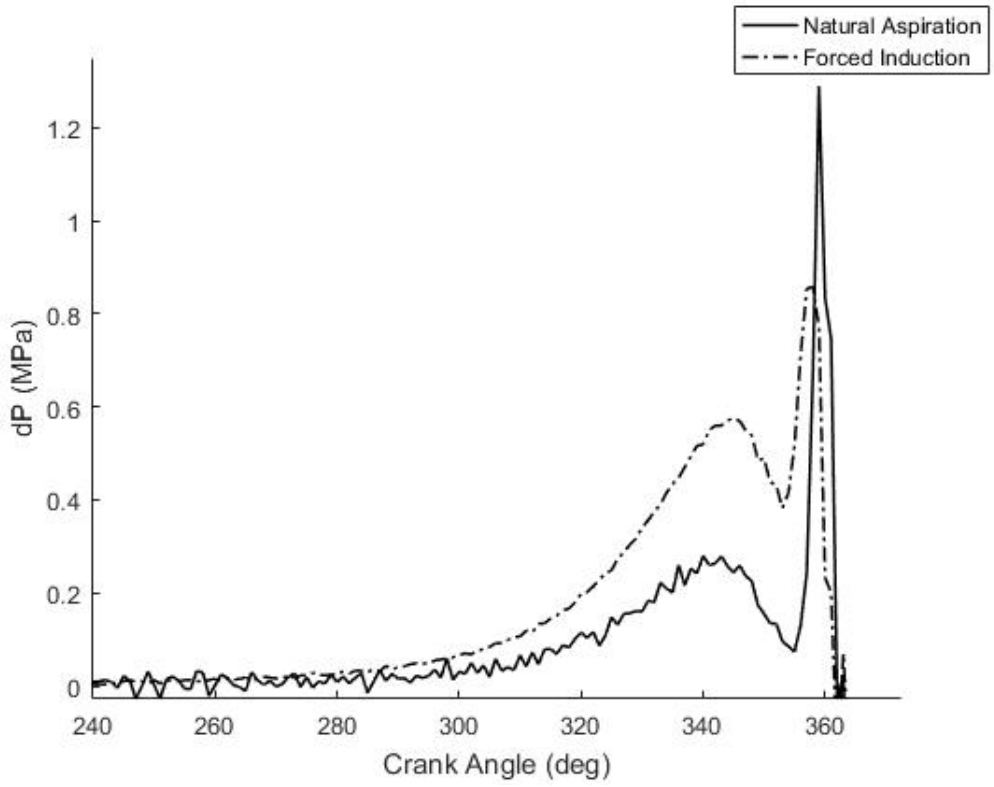

Figure 5.5: Comparison of the first derivative of cylinder pressure at 2500RPM, 6 ft-lb and 16 ^{o}BTDC.

Figure 5.6 shows the variation of cylinder pressure vs. crank angle with timing for 100% load (12 ft-lb) at 2000RPM.

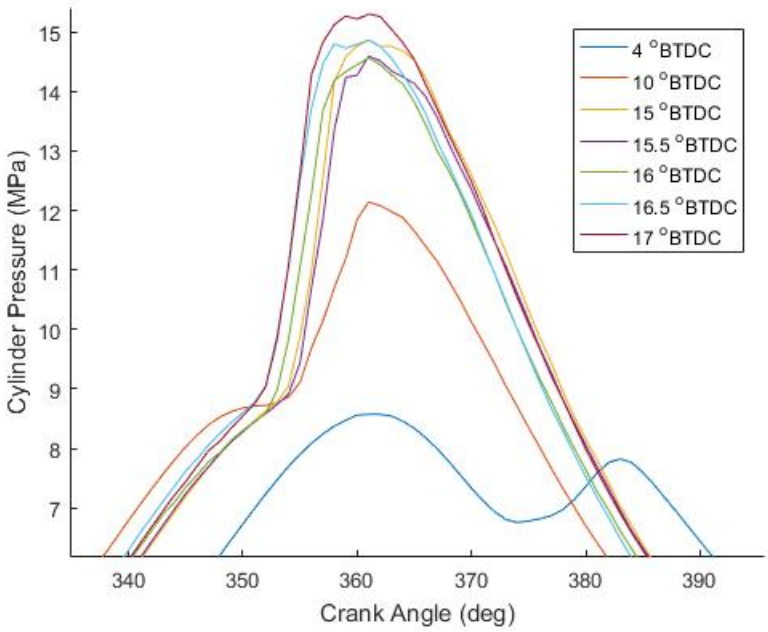

Figure 5.6: Cylinder pressure as a function of timing at 2000RPM and 12 ft-lb (natural aspiration).

From previous experience, the maximum cylinder pressure should reduce with timing retardation and this is confirmed by the traces shown in Figure 5.6. This is due to the fact that as timing is increasingly retarded, the piston is more likely to be moving towards bottom dead center (BDC) when combustion begins, which would result in a lower perceived cylinder pressure. It also shows that the two degree variation between 15 ^{o}BTDC and 17 ^{o}BTDC does not cause a significant change in cylinder pressure as the traces for those timings are within less than 1 MPa of each other.

One other thing that a wide range of timings affords is the inclusion of both pre-mix and diffusion combustion schemes. It can be observed that pre-mixing combustion increases with timing retardation. This is due to the fact that as timing is retarded, there is less time for the entire combustion event and as such, slower diffusion combustion is less likely to occur.

Temperature

Figures 5.7 and 5.8 show the variation of cylinder temperature vs. crank angle with torque.

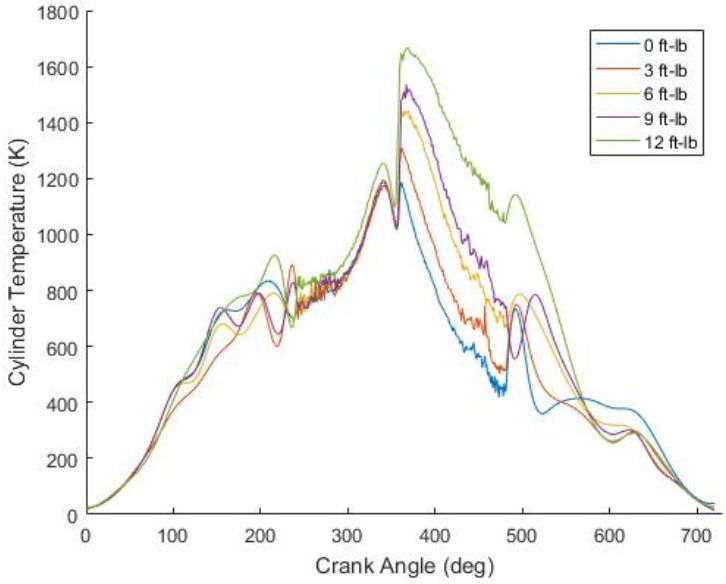

Figure 5.7: Cylinder temperature at 2500RPM and 16 ^{o}BTDC (natural aspiration).

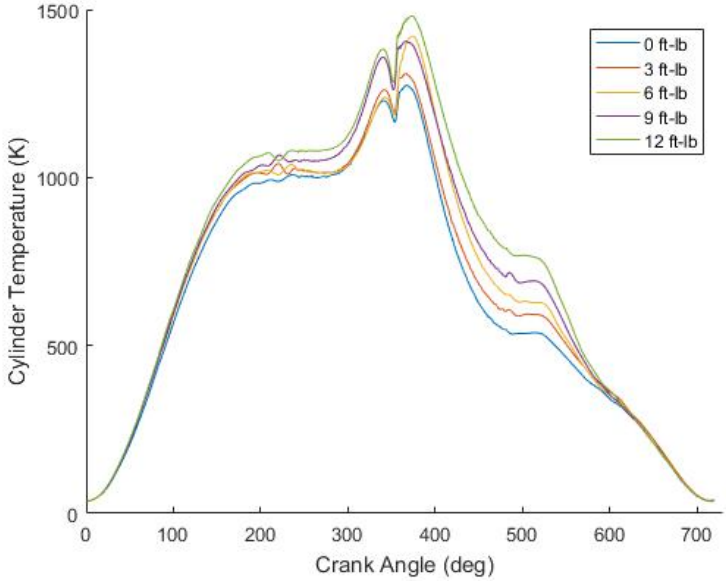

Figure 5.8: Cylinder temperature at 2500RPM and 16 ^{o}BTDC (forced induction).

As with the pressures, the cylinder temperatures can be seen to increase with load. The

ideal gas law can be used to explain why this is. The cylinder volume and gas constant are constant regardless of operating condition, but the cylinder pressure is shown to increase with load. The mass of fuel burned also increases with load, however, it is not proportional to the increase in pressure. This means that the temperature must also increase to keep the balance between both sides, leading to the trends observed.

Figure 5.9 shows a comparison between the cylinder temperatures between natural aspiration and forced induction.

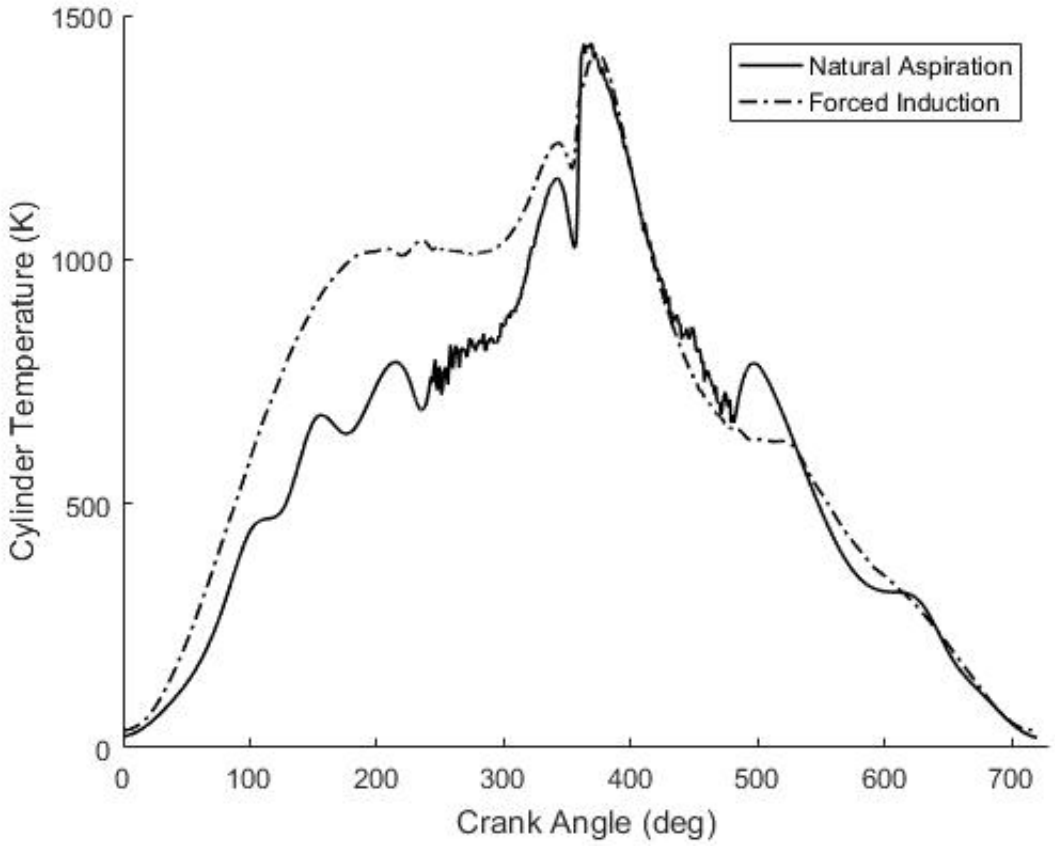

Figure 5.9: Comparison of cylinder temperature between natural aspiration and forced induction at 2500RPM, 6 ft-lb and 16 ^{o}BTDC.

Although not extremely evident from Figure 5.9, cylinder temperatures are generally lower for forced induction when compared to the equivalent operating condition for natural aspiration. This is due to the fact there is more denser, and by extension, colder air available

to cool down the contents of the cylinder as combustion progresses. Another trend that was observed was that the reduction in temperature increases with load. This means that at higher loads, the temperature reduction is much more evident. An example of a greater reduction in temperature is shown in Figure 5.10.

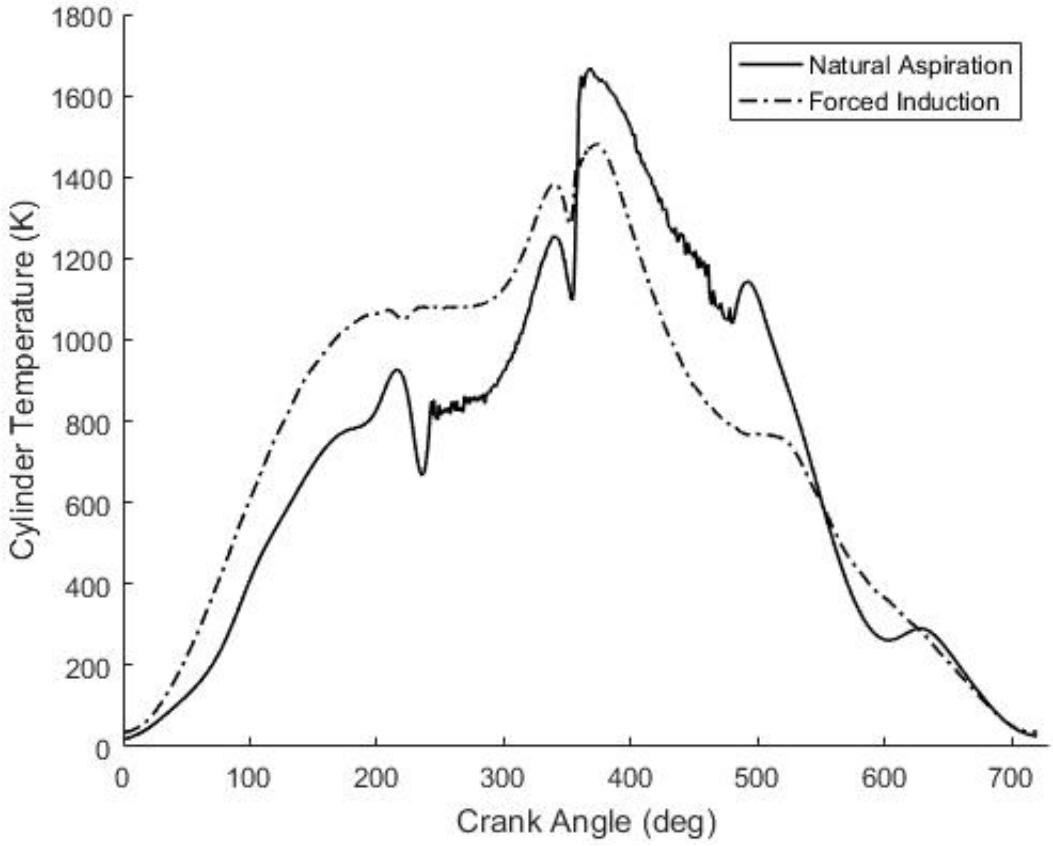

Figure 5.10: Comparison of cylinder temperature between natural aspiration and forced induction at 2500RPM, 12 ft-lb and 16 ^{o}BTDC.

From 5.11, it appears that extreme retardation increases the cylinder temperature. However, this would be incorrect as the reason the trace for 4 ^{o}BTDC is much higher than the others is because there is more fuel injected at that timing (17mg as opposed to an average of 14mg at the other timings). It is unclear as to why the maximum temperature for 10 ^{o}BTDC is lower than the other more advanced timings despite the fact that a similar amount of fuel is burned. Finally, as with the cylinder pressures the two degree

difference between 15 ^{o}BTDC and 17 ^{o}BTDC does not seem to cause a significant change in temperature as the traces are within $\sim$50K of each other.

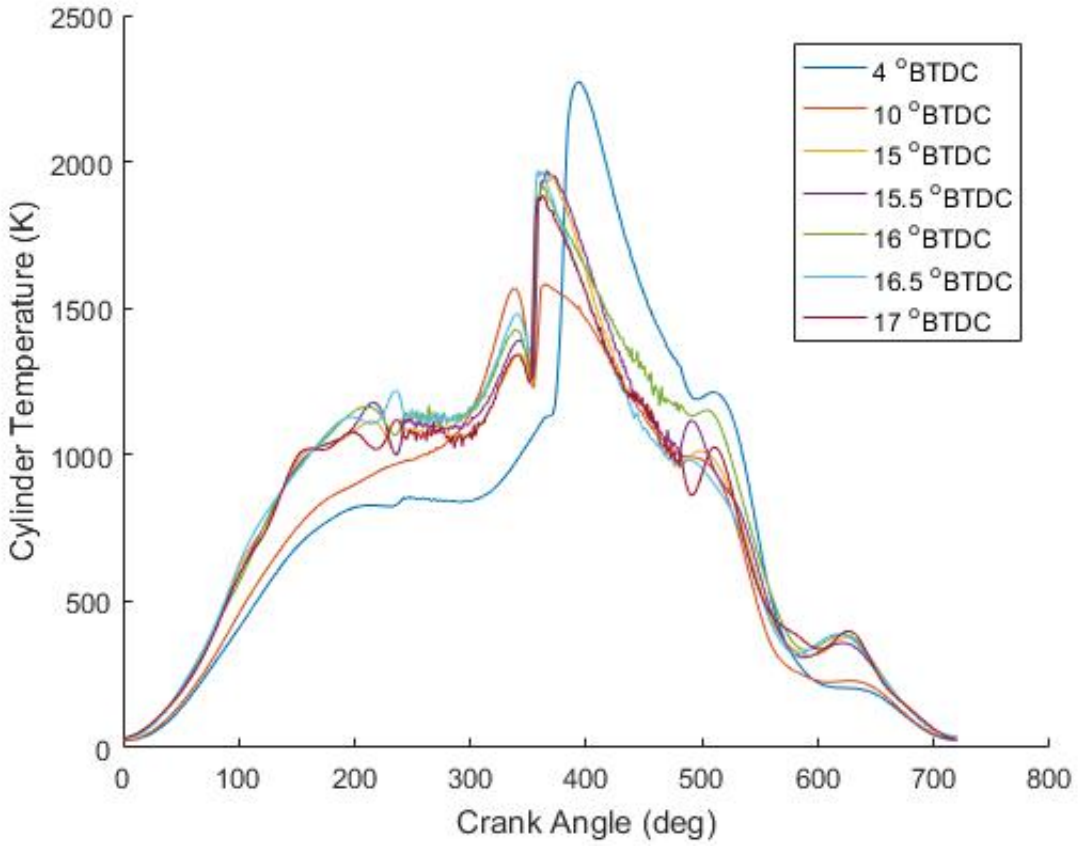

Figure 5.11: Cylinder temperature as a function of timing at 2000RPM and 12 ft-lb (natural aspiration).

The cylinder temperature is not the only temperature that changes with timings. As it turns out, the exhaust temperature changes as well. As with the cylinder temperature, it would be expected that the exhaust timing would follow a similar trend. This is confirmed by Figure 5.12.

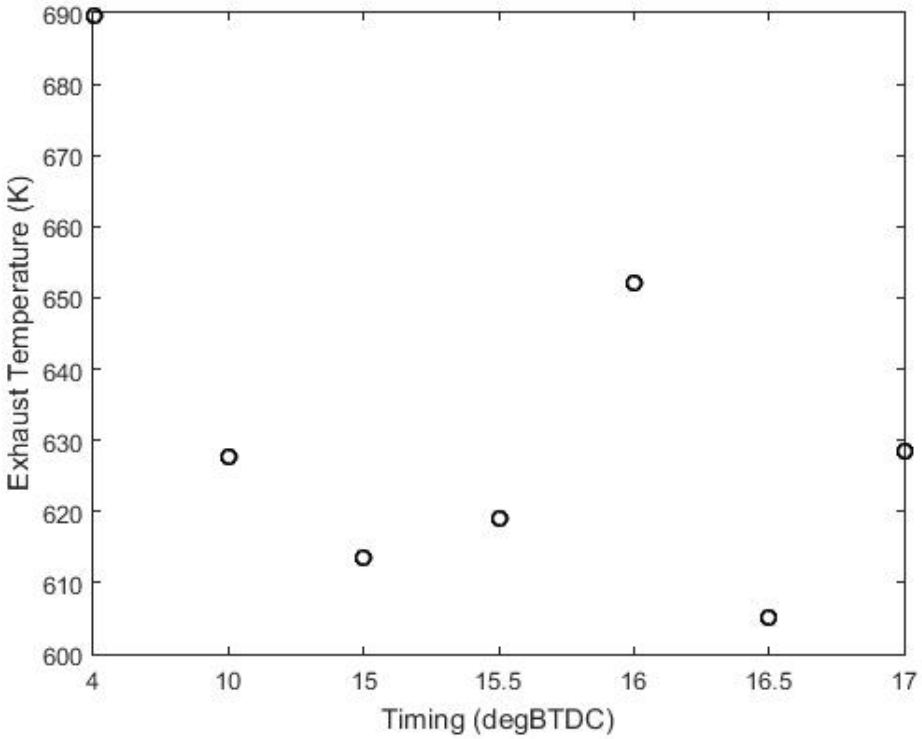

Figure 5.12: Exhaust temperature as a function of timing at 2000RPM and 12 ft-lb (natural aspiration).

Heat Release Rate

Figures 5.13 and 5.14 shows the variation of the net heat release rate vs. crank angle with torque for natural aspiration and forced induction.

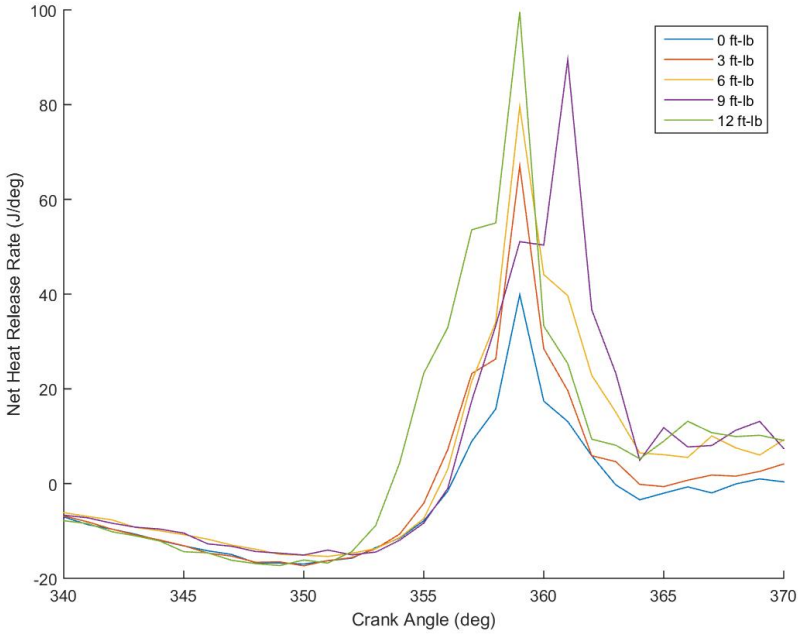

Figure 5.13: Net heat release rate at 2500RPM and 16 ^{o}BTDC (natural aspiration).

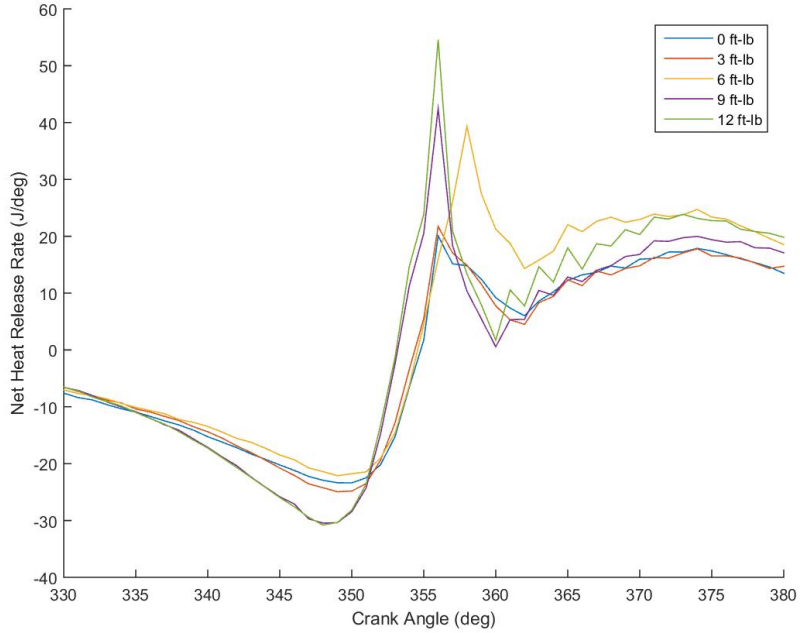

Figure 5.14: Net heat release rate at 2500RPM and 16 ^{o}BTDC (forced induction).

It would be expected that the rate of heat release would increase as the load is increased

as there is more fuel being combusted at the higher load levels. From Figures 5.13 and 5.14, it can be seen that this trend is observed regardless of injection scheme. It is unclear as to why the maximum values of some curves are shifted to the right.

The net heat release rate is the total rate of fuel energy added to the cylinder as combustion progresses. However, as the actual heat release rates cannot be directly determined, the term *apparent* is sometimes used as a descriptor. In addition, the traces shown actually represent the apparent net heat release rate which is the apparent gross (total) heat release rate minus the heat lost through the cylinder walls.

The maximum value spike is caused by the thermodynamics of premix combustion which registers within the measured engine parameters. However, looking at Figures 5.13 and 5.14, it can be seen that there is a dip below zero before the spike. This seems like an anomaly as fuel is being combusted which should always cause a large amount of heat to be released. The explanation is much simpler than that: the dip is caused by the fuel evaporating right after it is injected into the cylinder. After the fuel is injected, it absorbs heat and starts to evaporate, which causes an apparent negative release of heat which manifests as the dip in the trace.

Figure 5.15 shows a comparison of heat release rates between natural aspiration and forced induction.

It seems odd that forced induction would have a lower heat release rate than the natural aspiration as shown in Figure 5.15. Normally, the point of forced induction is to force more air into the engine, that way, more fuel can also be injected (keeping AFR relatively constant) to increase the amount of power that the engine can produce. If that was the case, then the trend shown in Figure 5.15 would be troubling.

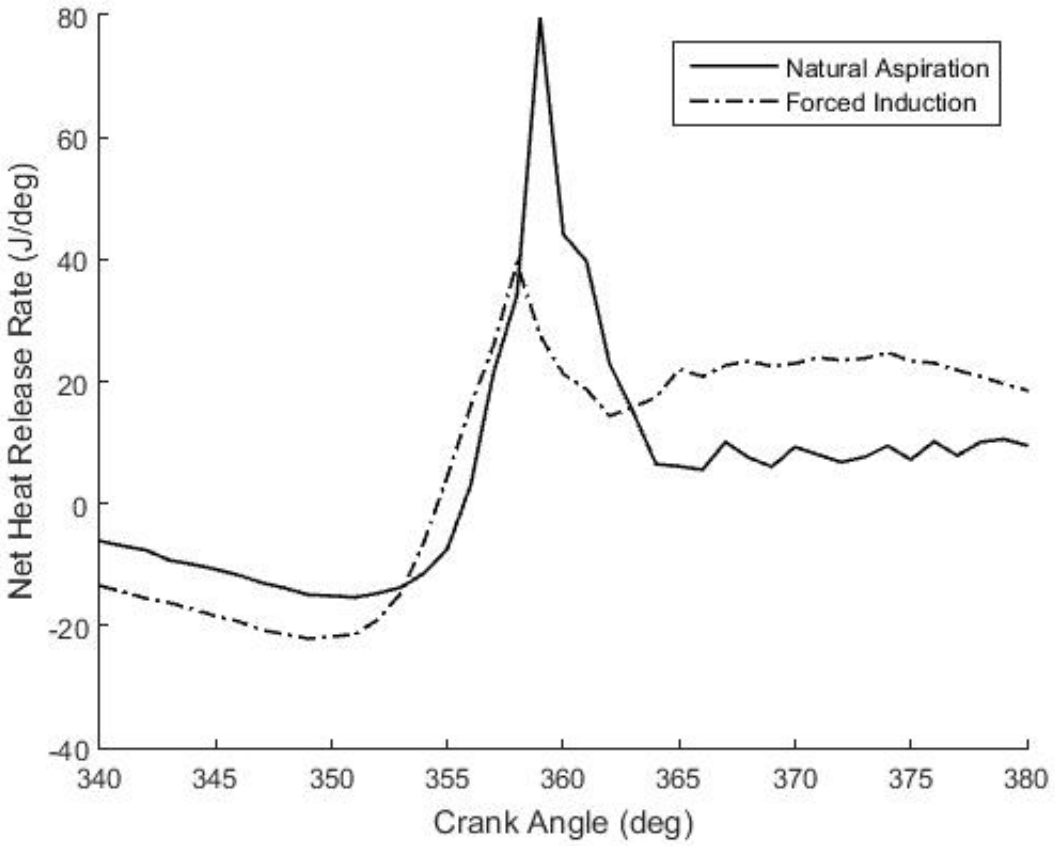

Figure 5.15: Comparison of net heat release rate between natural aspiration and forced induction at 2500RPM, 6ft-lb and 16 ^{o}BTDC.

However, the forced induction scheme employed in this study does not increase the amount of fuel with the increased amount of air. In essence, the combustion event is being extremely leaned out and AFR is greatly increased. It is this change that causes the trend in Figure 5.15 to make sense. There is just so much air cooling that the rate at which the heat from the burned fuel can be added to the contents of the cylinder is reduced relative to the equivalent natural aspiration operating point. This is also touched on in the temperature discussion as the cylinder temperatures are generally lower for forced induction. In addition to all this, Figure 5.15 confirms the fact that forced induction produces a more diffuse combustion than natural aspiration.

As discussed, the net heat release rate is the incremental energy released as the fuel

is combusted. To find the total amount of heat released, the cumulative heat release rate is calculated. The cumulative heat release is the integral of the net heat release rate and can be calculated as the summation of the net heat release rate values over each crank degree as combustion progresses.

Figures 5.16 and 5.17 show the variation of the cumulative heat release vs. crank angle as a function of torque for natural aspiration and forced induction.

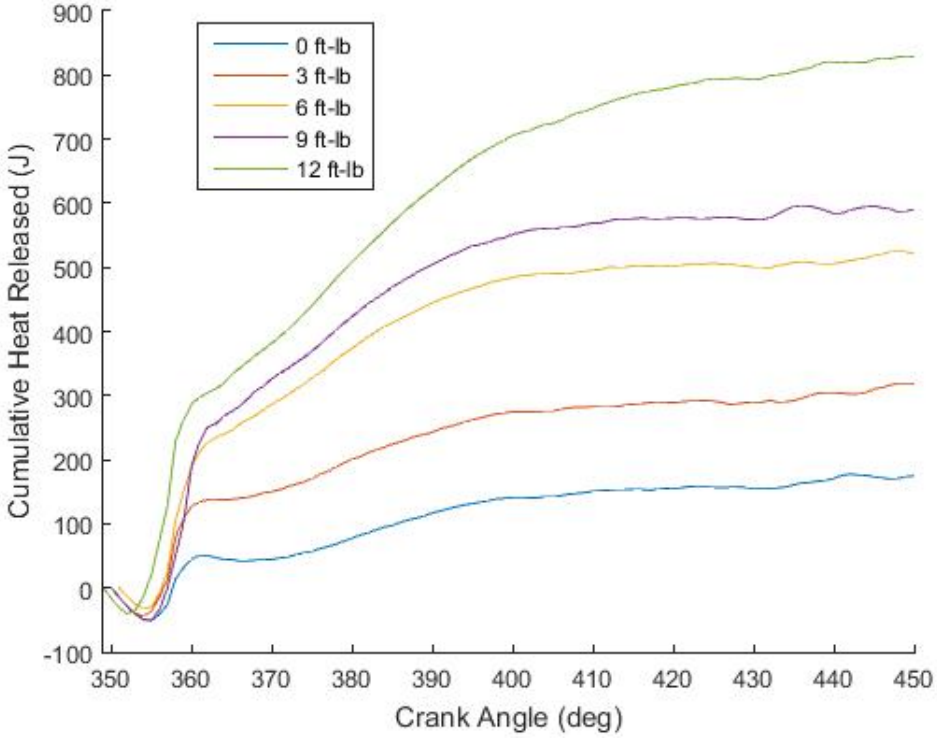

Figure 5.16: Cumulative heat release at 2500RPM and 16 ^{o}BTDC (natural aspiration).

Figures 5.16 and 5.17 show an increase in the total amount of heat released as load increases. This is a trend that has been observed with other engine combustion parameters and is also independent of injection scheme.

Figure 5.18 shows a comparison of cumulative heat release between natural and forced induction.

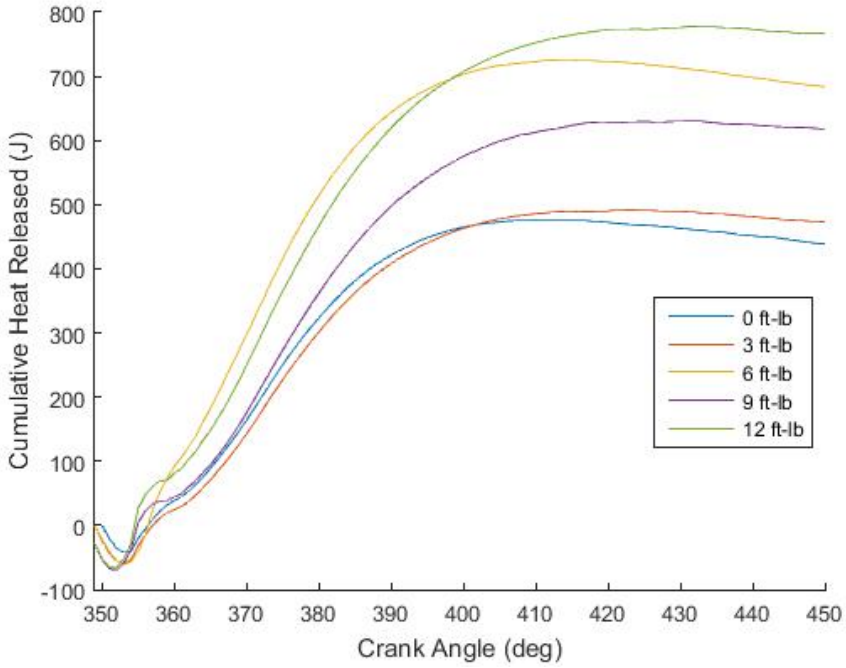

Figure 5.17: Cumulative heat release at 2500RPM and 16 ^{o}BTDC (forced induction).

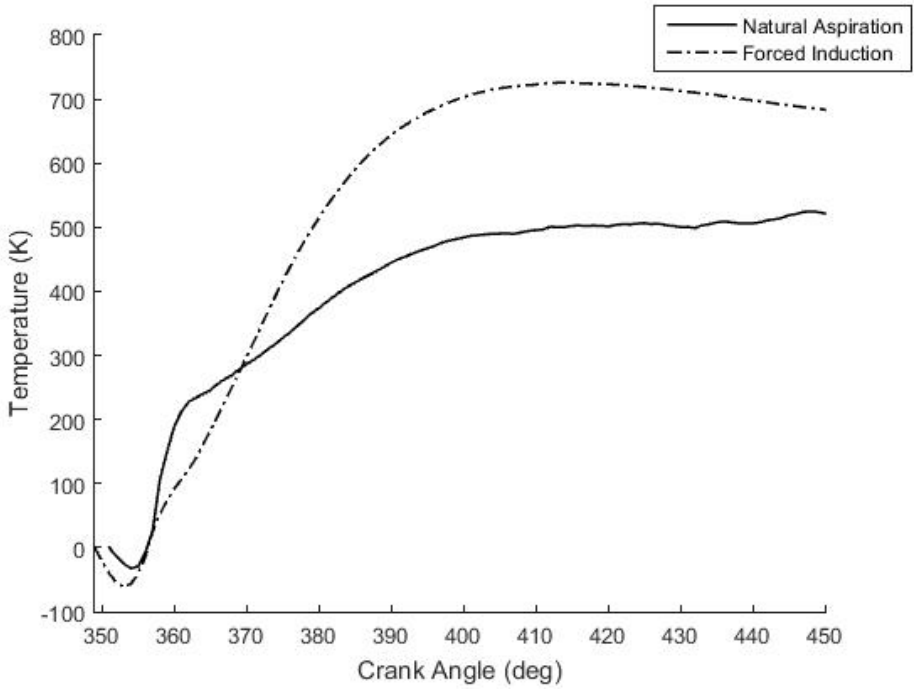

Figure 5.18: Comparison of cumulative heat release between natural aspiration and forced induction at 2500RPM, 6ft-lb and 16 ^{o}BTDC.

Seeing as the net heat release was lower for the forced induction scheme, it seems backwards that it would show the higher amount of cumulative heat released in Figure 5.18. Looking at Figure 5.15, it can be seen that trace for natural aspiration drops back down to nearly zero after the spike which suggests that there is little diffusion combustion happening. Even though the trace for forced induction does not have as large of a spike, it compensates by releasing heat for a longer time after the spike when compared to natural aspiration. It means that the forced induction scheme on average is releases more heat over the same combustion event than the natural aspiration scheme.

5.2 PN Concentration

The first particulate number (PN) result that will be discussed in the PN concentration. This is the output from the engine exhaust particle sizer (EEPS) and describes the number of particles in a given volume of exhaust across all measured particle diameters.

Figure 5.19 shows the PN concentration distribution for natural aspiration at 15 ^{o}BTDC, 0 ft-lb and 2000RPM. Note that the displayed concentrations are 16 times higher than the actual levels.

It can be seen that the concentration shows a decrease in the smaller particles as load is increased. This reduction in the smaller particles is accompanied by an increase in larger particles, which gets more pronounced at the highest load levels. This is consistent with anecdotal evidence as a diesel producing a high torque has been known to emit more smoke than one producing a lower torque.

Figure 5.20 shows the PN concentration distributions for forced induction at 15 ^{o}BTDC, 0 ft-lb and 2000RPM.

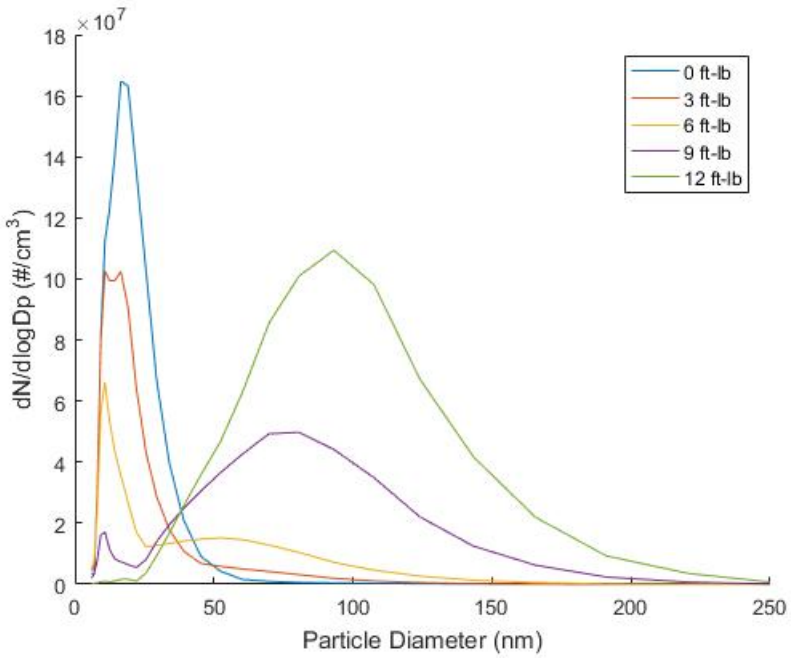

Figure 5.19: PN concentration distribution across particle diameters for natural aspiration.

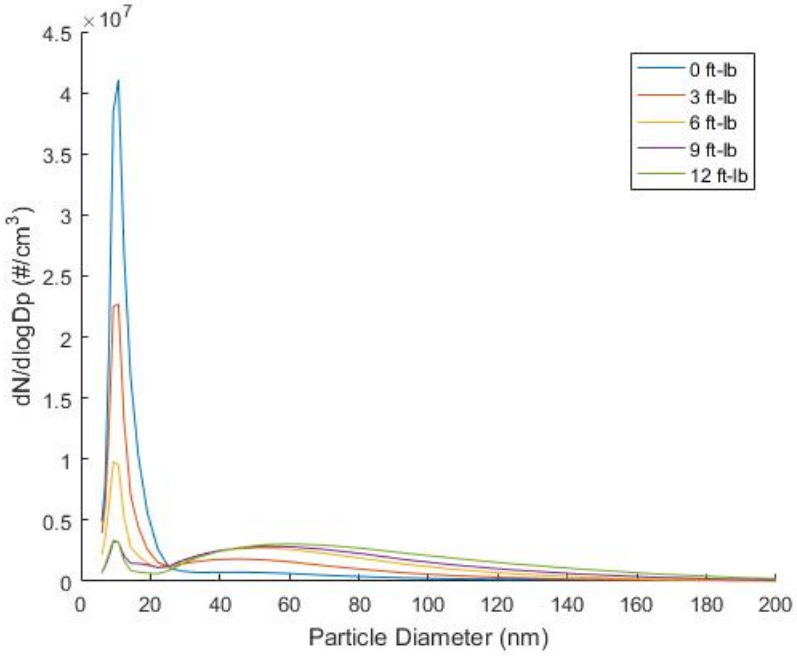

Figure 5.20: PN concentration distribution across particle diameters for forced induction.

The first thing of note is that forced induction slightly reduces the concentration as it can be seen that there is roughly a four times reduction in concentration across all loads.

From Figure 5.20, it can be seen that there is the same decrease in smaller particles that was observed in Figure 5.19. However, the rightward shift, while still present, has been greatly reduced (approximately a 24 times reduction). As mentioned earlier, increasing the AFR causes a massive reduction in smoke which implies that the reduction in smoke is correlated to the reduction in concentration of the larger particles that would normally be present in the exhaust under natural aspiration. This gives us the answer to the question: If smoke levels decrease with increased AFR, what happens to PN?

The second thing to note from Figures 5.19 and 5.20 is that the concentration distribution appears to be bimodal. This is best shown by the 9 ft-lb trace for natural aspiration as there appear to be two distinct peaks separated at $\sim$20nm.

It is possible that the first mode comes from complex solid particle nucleation modes as reported by Filippo and Maricq [63]. Another possibility is that the hot dilution did not fully condition the sampled exhaust stream and volatiles were still present. However, it is known that this is not the case as the thermodiluter and thermal conditioner work in tandem to heat the sample to high temperatures (300^{o}C) to ensure the complete evaporation of volatiles in the sample stream. The third reason is that the bimodality is caused by the evaporation of lubricating oil used within the engine. This conclusion can be drawn because Czerwinski et al. have shown that the evaporation of lubricating oil does have an effect on the particulate emissions from an engine [64].

The bimodality is even more clear if the concentrations are segregated about that 20nm bimodal point. Figures 5.21 and 5.22 show these segregated concentrations for both natural aspiration and forced induction at 17 ^{o}BTDC for all loads.

Figures 5.21 and 5.22 confirm the bimodality as there are two clear and consistent trends for each mode. In addition, they lend more credence to the fact that the smoke reduction is due to the reduction of the concentration of large particles in the exhaust.

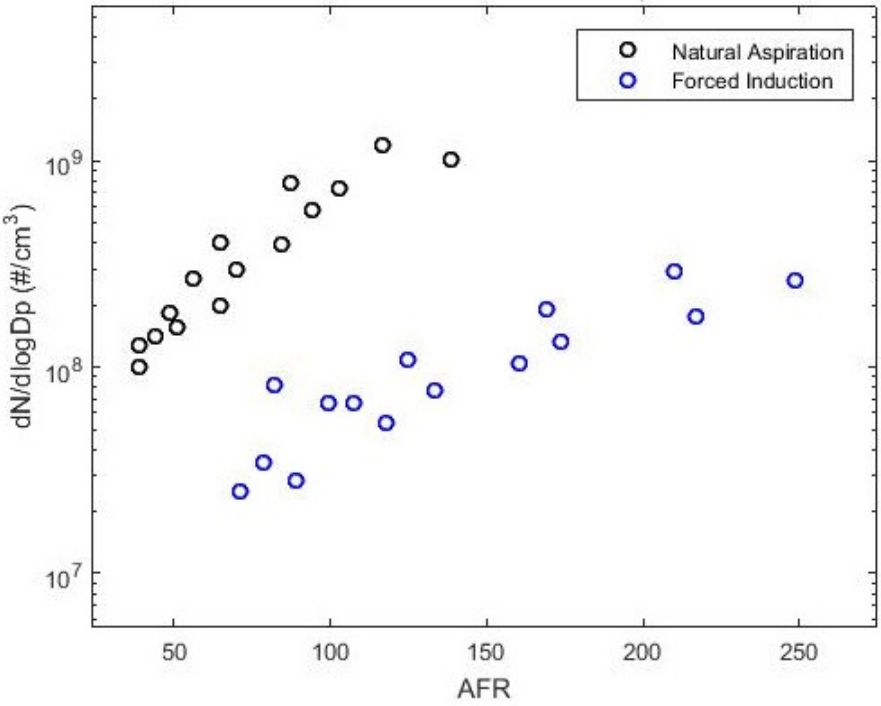

Figure 5.21: Concentration comparison at 17 ^{o}BTDC for d_p < 20nm.

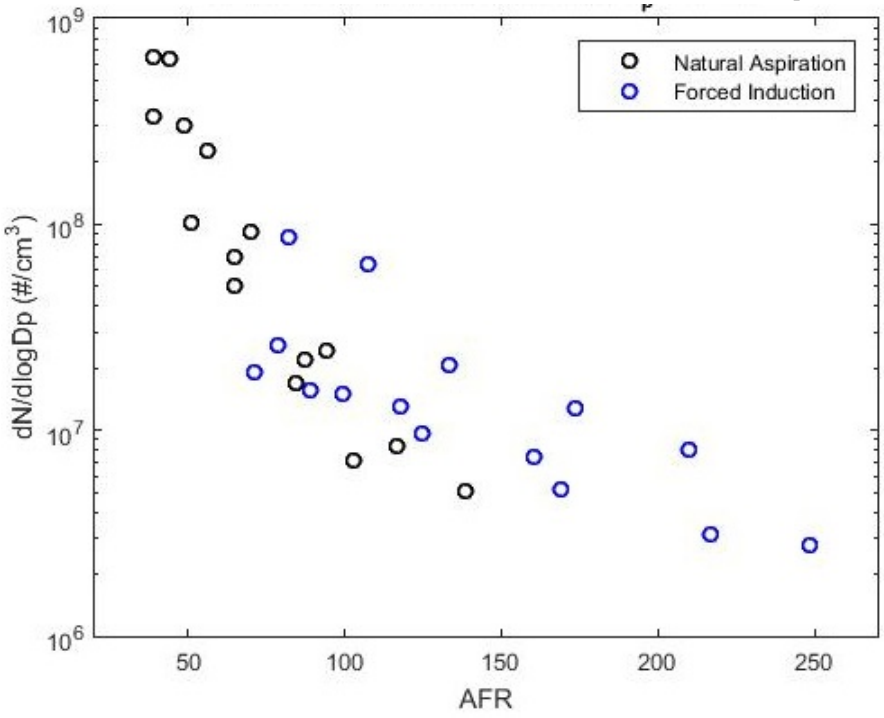

Figure 5.22: Concentration comparison at 17 ^{o}BTDC for d_p > 20nm.

5.3 Oil Study

As mentioned in the previous section, the two possible causes for the bimodality are complex solid particle nucleation modes and the lubricating oil. However, the first reason is beyond the scope of the work presented in this thesis and cannot be tested. Since oils of different formulations are readily, cheaply available, a simple oil study was performed to check whether or not a variation in the lubricating oil would have an effect on the measured PN concentrations.

Three oils were used in this study, a conventional (mineral) SAE-30 oil that was formulated for diesel fleet vehicles, a fully synthetic 10W-30 oil with a large amount of additives, also formulated for diesel engines, and a synthetic 10W-30 oil blend designed for gasoline engines.

Naturally aspirated 6 ft-lb, 2500 RPM at 16 ^{o}BTDC was chosen as the single operating test point as it is exactly in the middle of the two degree timing range. Forced induction was not tested as it was decided to keep the amount of variables to a minimum.

Figure 5.23 shows the total PN concentration distribution for the three oils.

Above 20nm, Figure 5.23 shows negligible differences in PN concentration between the oil formulations. Below 20nm, it can be seen that the fully synthetic diesel oil shows the highest concentration, $\sim$3 times higher than either of the other two oils. In addition, the conventional diesel oil behaved fairly similarly to the gasoline formulation.

To further show this difference about the bimodal point, the distribution was segregated about 20nm and shown in Figure 5.24.

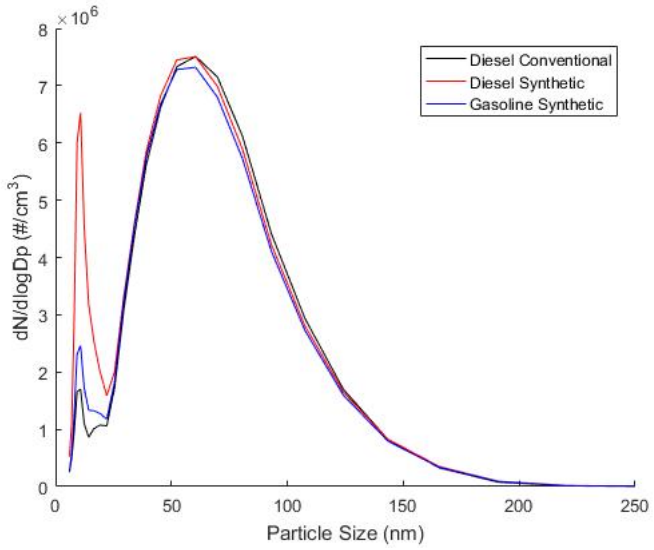

Figure 5.23: Comparison of different oils at 6 ft-lb, 2500 RPM and 16 ^{o}BTDC (natural aspiration).

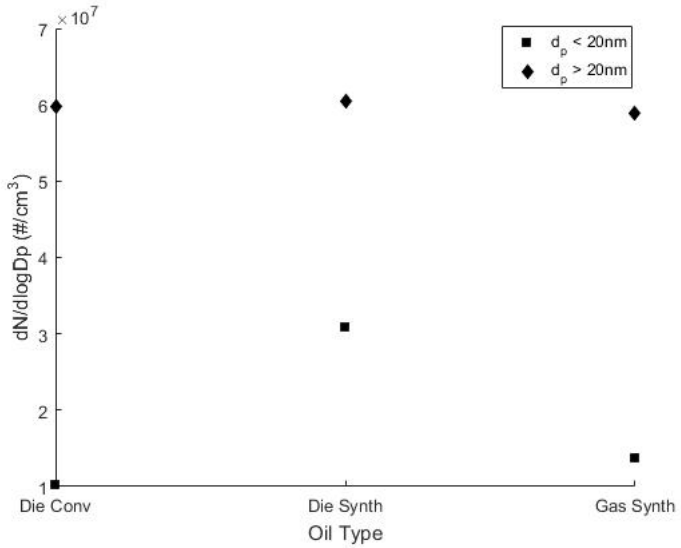

Figure 5.24: Segregated comparison of the different oils at 20nm for 6 ft-lb, 2500 RPM and 16 ^{o}BTDC (natural aspiration).

Figure 5.24 shows that for particles with diameters greater than 20nm, the trend is fairly straight across the oil types, while for particles with diameters less than 20nm, the synthetic diesel oil shows a higher concentration.

To push the oil study to its extreme, it was decided to see how the PN concentration

would change as the lubricating oil was removed from the engine while it was running. This turned out to not be feasible as the engine employs a splash system that caused the oil to come out in spurts making a timely collection of the data impossible. It was then decided to remove the oil from the engine and test the dry setup at the same load-speed-timing combination.

About a minute and a half of data was obtained before friction losses were too great and the engine stopped, but that data allows a comparison between having oil in the engine and having no oil. Figure 5.25 shows a comparison in the overall distribution between oil and no oil.

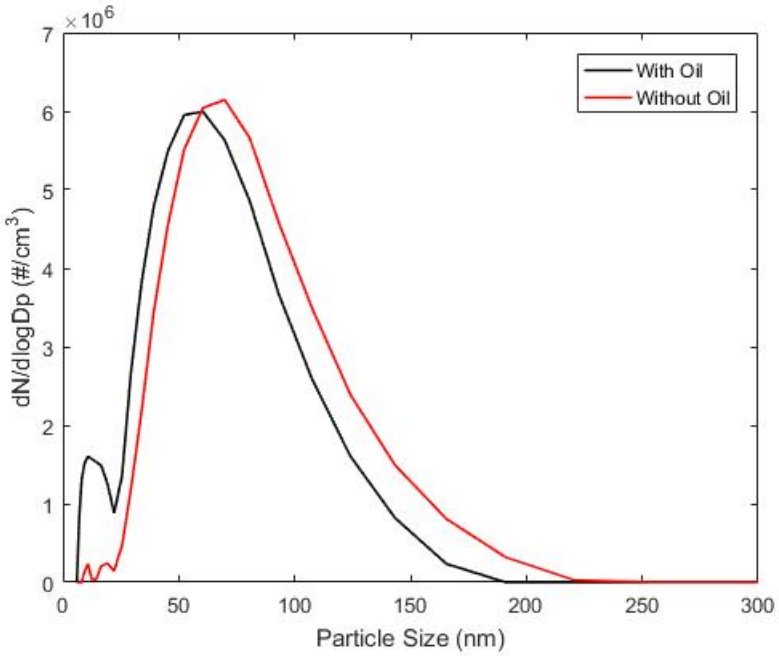

Figure 5.25: PN concentration for oil vs. no oil at 176 for 6 ft-lb, 2500 RPM and 16 ^{o}BTDC (natural aspiration).

Figure 5.25 shows that at steady state, there is little difference between the oil and no oil concentrations for particle diameters above 20nm. However, it can also be seen that there are negligible amounts of sub-20nm particles present when the oil is removed from the engine.

When combined with the fact that the oil comparison shows only changes in sub-20nm

concentrations, it would be easy to conclude that the oil is in fact causing the bimodal distribution. Even if this were true, it should be noted that this study is not comprehensive and cannot confirm that fact on its own. It was performed to determine whether oil formulation (or lack thereof) has an effect on PN concentration, and the traces tend to show that it does. Despite that, PN production mechanisms are more nuanced than this simple oil study suggests, so further, more in-depth testing would have to be performed in the future to check how exactly the chemical makeup and physical properties of the oil affect the PN concentration, and whether or not there is some other variable causing the observed changes.

5.4 Energy Specific PN

Energy specific PN is the PN concentration normalized by the energy produced by the engine. This was done to reduce potential fluctuations in the raw concentrations and produce a more stable comparative result.

Figure 5.26 shows a comparison of energy specific PN for 17 ^{o}BTDC at all loads.

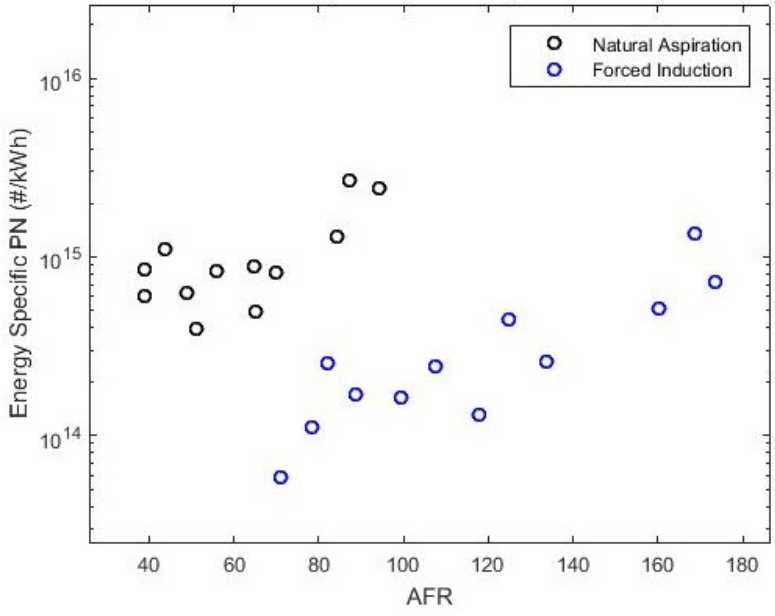

Figure 5.26: Energy specific PN comparison at 17 ^{o}BTDC.

From Figure 5.26, it would appear that there is a slight increase in energy specific PN with AFR but the values are generally in the same range for both natural aspiration and forced induction.

Figure 5.27 shows a comparison of energy specific PN across all timings for 2000RPM.

While the slight increase observed in Figure 5.26 is also present in Figure 5.27, the values are once again within the same range. This suggests that timing may not have an effect on the energy specific PN produced by the engine.

As with the concentration data, the energy specific PN was segregated about the 20nm bimodal point and the results are shown in Figures 5.28 and 5.29.

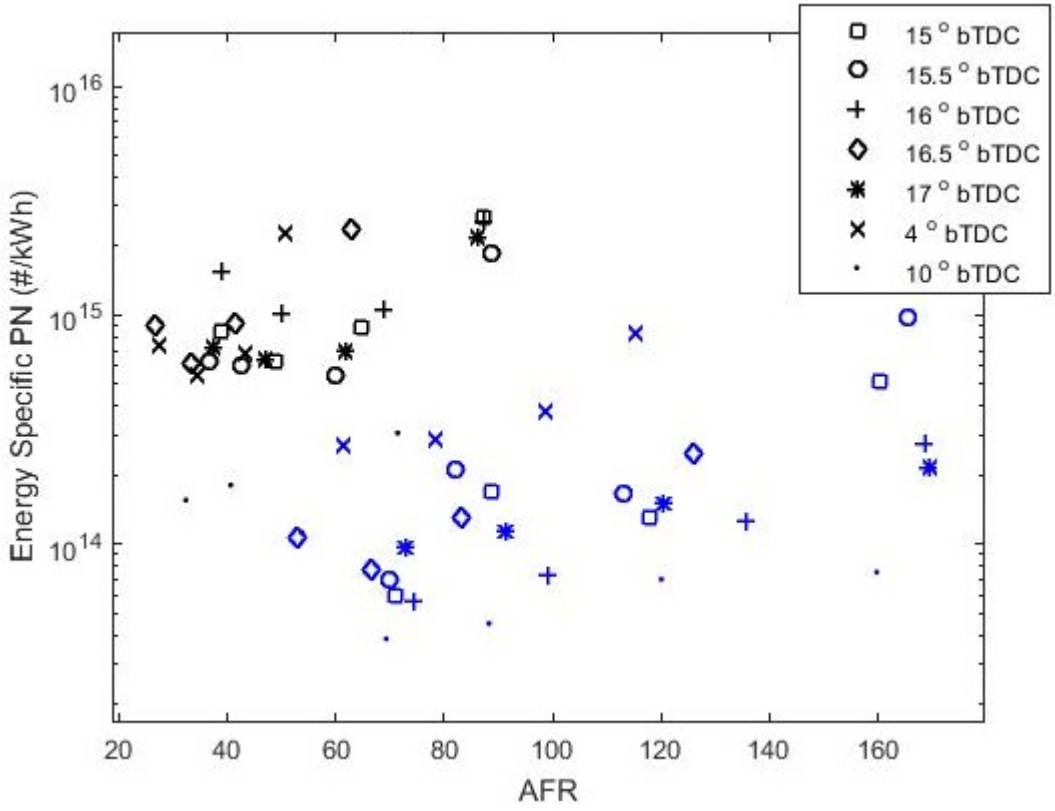

Figure 5.27: Energy specific PN comparison across all timings at 2000RPM.

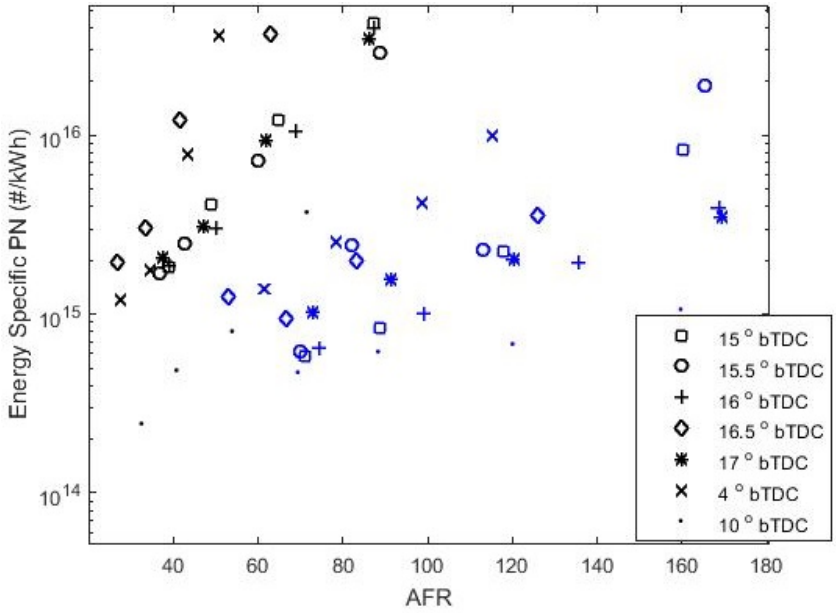

Figure 5.28: Energy specific PN comparison across all timings at 2000RPM for $d_p < 20$nm.

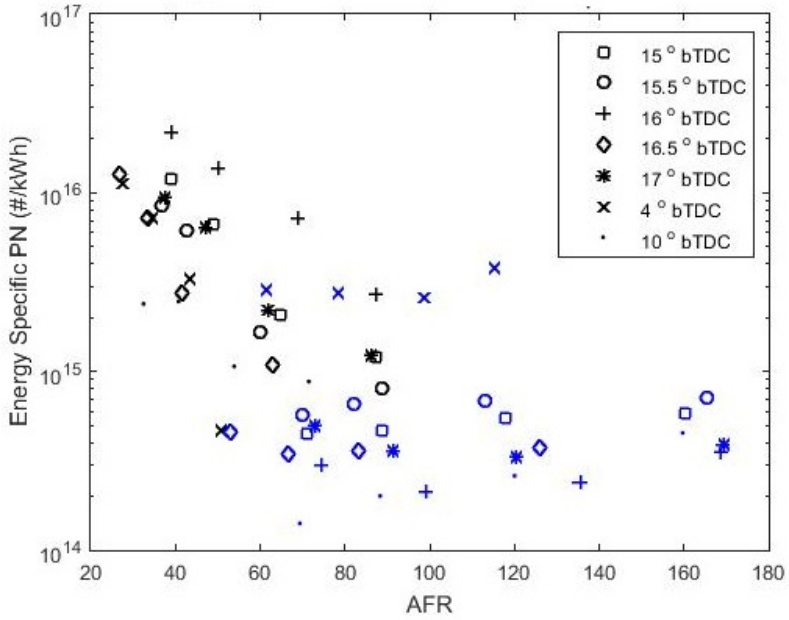

Figure 5.29: Energy specific PN comparison across all timings at 2000RPM for $d_p > 20$nm.

The same general trend is observed here with the particles with diameters under 20nm show an increase with AFR and particles above 20nm show a decrease. This once again strengthens the claim that smoke reduction is due to a reduction in the amount of large particles present.

5.5 PN Production Rate

The PN production rate is the PN concentration normalized by the exhaust flow rate. This allows the determination of how much PN is being produced by the engine at a given operating point per hour.

Figure 5.30 shows a comparison of the PN production rate for 17 ^{o}BTDC at all loads.

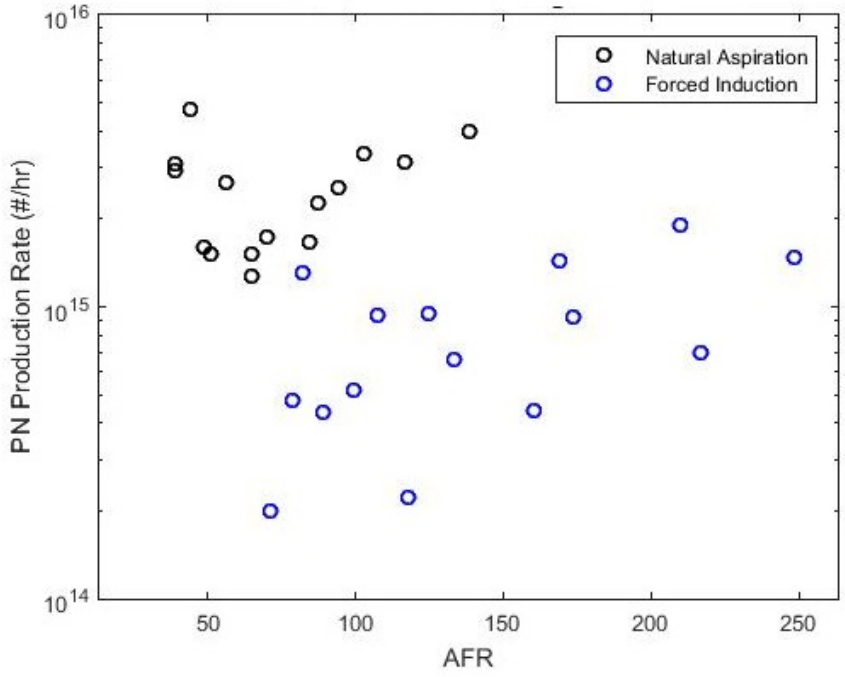

Figure 5.30: PN rate comparison at 17 ^{o}BTDC.

Similarly to energy specific PN, the PN production rates seem to increase slightly with AFR, while all being in the same range.

Figure 5.31 shows a comparison of PN production rate across all timings for 2000RPM.

Figure 5.31 seems to show no increase nor decrease across the AFR range as it is fairly horizontal. As with the energy specific timing comparison, timing does not seem to have an effect on the PN production rate as the values are all within one order of magnitude of each other.

To see effects of the bimodality, the PN production data was also segregated about particle diameter of 20nm and Figures 5.32 and 5.33 show the graphs.

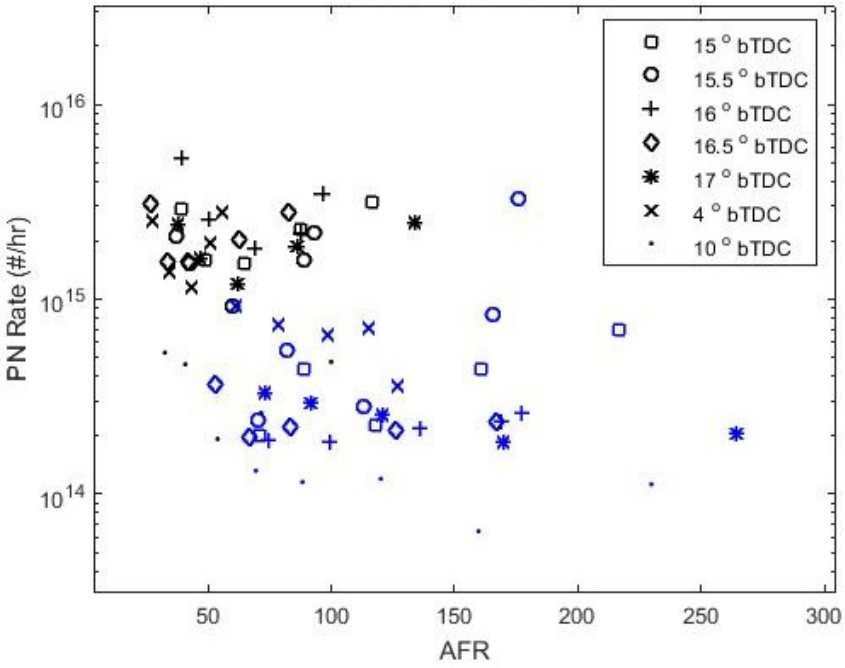

Figure 5.31: PN rate comparison across all timings at 2000RPM.

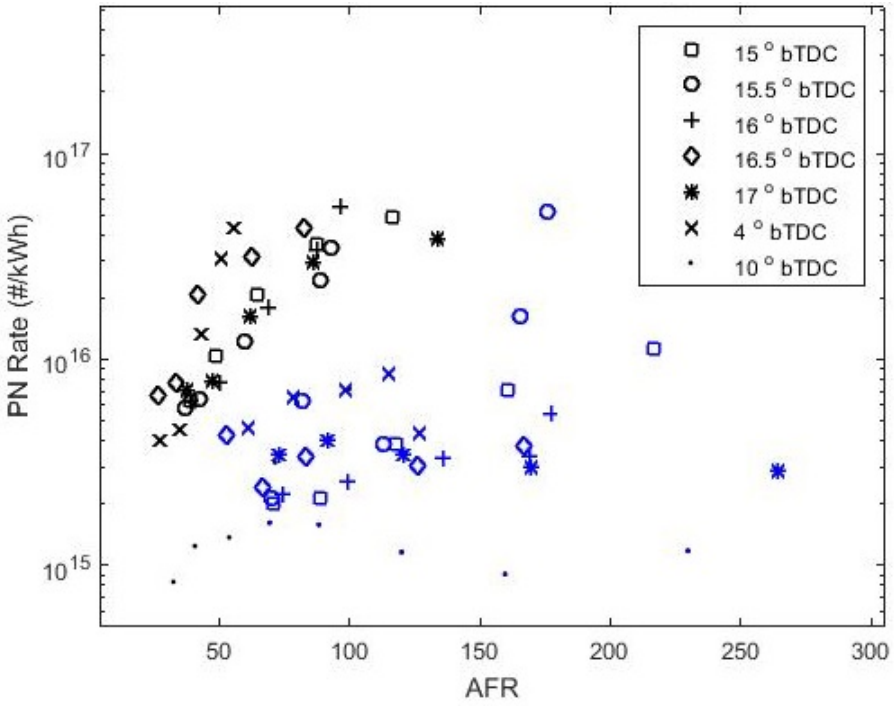

Figure 5.32: PN rate comparison across all timings at 2000RPM for $d_p < 20$nm.

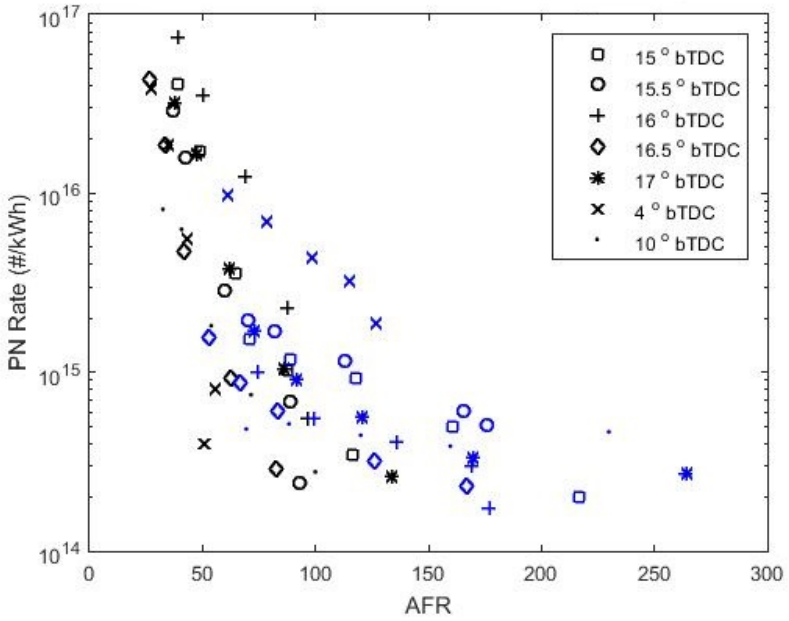

Figure 5.33: PN rate comparison across all timings at 2000RPM for $d_p > 20$nm.

As with the segregated data for PN concentration and energy specific PN, the PN production rate also shows an increase in sub 20nm particles with AFR and a reduction in the production of particles with diameters above 20nm. This means that there are less larger particles present in the exhaust because the engine is producing less of them at the higher AFR values.

Chapter 6

CONCLUSION

Using the results of the PN analysis, it has been shown that increasing the AFR reduces the overall presence of larger particles in the exhaust stream which is observable as a reduction in the amount of smoke detected. In addition, looking at each of the modes of the particle number (PN) data separately, reinforces that notion because a clear decrease is seen in the large particles accompanied by an increase in the concentration of smaller particles due to the interaction of the injected air and lubricating oil.

The bimodality of the concentration was investigated and it was found that the lubricating oil has a significant effect on the sub-20nm mode of the distribution. This is evidenced by the fact that changing the formulation of the oil also caused the concentration of sub-20nm nuclei particles to change, and removing the oil from the engine resulted in a substantial reduction. All these changes were observed while the larger particle (d_p > 20nm) mode stayed relatively constant across the tests.

The engine is this study had an energy specific particle number of between 10^{14} (forced induction) #/kWh and 10^{15} (natural aspiration) #/kWh which is within the range published in literature [65]. This indicates that using a diesel particulate filter (DPF) as an after-treatment on the exhaust stream makes it possible to bring the values of the test cell

down to levels which are within the EURO standards.

Starting off with speed and load, it does not appear that changing the speed and load has any effect on the energy specific PN or PN production rate. However, if only one timing is looked at, there appears to be a slight increase in the energy specific PN and PN rate with a reduction in speed and load. Despite this, the values are all within the same range so the effects of speed and load are negligible.

There is about a doubling in the AFR between natural aspiration and forced induction for a given speed-load-timing condition, but that only results in less than one order of magnitude difference in the energy specific PN and PN production rate. This is not a substantial change because the reduced value of 10^{14} #/kWh is still a very large number of particles.

Lastly, varying the timing allows the exploration of both diffusion burn and pre-mixed combustion. However, even this does not seem to have an effect on the amount of PN produced as the data is jumbled up for all the timings within the same order of magnitude indicating a negligible difference.

What this suggests is that operating condition does not have a significant effect on the levels of PN produced from the engine implying that there is no way to reduce the amount of PN by simply changing operating point. While the historical practice of increasing the AFR reduces the amount of smoke to unmeasurably low levels, it simply changes the structural makeup of the PN while still leaving it measurable and relatively unchanged. It would appear that the only reliable way to reduce PN levels is to use a DPF despite the fact that it might increase the cost and complexity of the engine.

References

[1] Heywood J.B. *Internal Combustion Engine Fundamentals*. McGraw-Hill, 1988, pp. 1–7.

[2] Hills R.L. *Power from Steam*. Cambridge University Press, 1989, pp. 1–13.

[3] Heywood J.B. *Internal Combustion Engine Fundamentals*. McGraw-Hill, 1988, pp. 15–19.

[4] Heywood J.B. *Internal Combustion Engine Fundamentals*. McGraw-Hill, 1988, pp. 25–31.

[5] Heywood J.B. *Internal Combustion Engine Fundamentals*. McGraw-Hill, 1988, pp. 45–53.

[6] Schifsky C., ed. *Tech: Gas vs. Diesel. Which is best for you?* Mar. 2002. URL: http://www.trucktrend.com/how-to/expert-advice/163-0210-diesel-vs-gas/.

[7] *Most Powerful Pre-War Cars*. July 2010. URL: http://oppositelock.kinja.com/most-powerful-pre-war-cars-1716899732.

[8] *Bugatti Chiron Overview*. URL: https://www.bugatti.com/chiron/.

[9] Neff J., ed. *Engine power has increased 112% since 1980 and other fun facts about the Horsepower Wars*. May 2010. URL: https://www.autoblog.com/2010/05/25/horsepower-has-increased-112-since-1980-and-other-fun-facts/.

[10] Brad Tuttle, ed. *What, You Only Have 100K Miles on Your Car? That's Nothing*. Mar. 2012. URL: http://business.time.com/2012/03/20/what-you-only-have-100k-miles-on-your-car-thats-nothing/.

[11] *Tier 4 Engine Classification*. URL: https://www.dieselnet.com/standards/us/nonroad.php#tier4.

[12] Heywood J.B. *Internal Combustion Engine Fundamentals*. McGraw-Hill, 1988, pp. 5–7.

[13] Haagen-Smit A.J. "Chemistry and physiology of Los Angeles smog". In: *Industrial and Engineering Chemistry* 44.6 (1952), pp. 1342–1343.

[14] Canakci M. and Van Gerpen J.H. "Comparison of engine performance and emissions for petroleum diesel fuel, yellow grease biodiesel, and soybean oil biodiesel". In: *American Society of Agricultural Engineers* 46.4 (2003), pp. 937–944.

[15] Turns S.R. *An Introduction to Combustion. Concepts and Applications*. 3rd ed. McGraw-Hill, 2012, p. 21.

[16] *Fact Sheet: What you need to know about Carbon Monoxide*. 2016. URL: https://www.health.ny.gov/environmental/indoors/air/carbon_monoxide_need_to_know.htm.

[17] Ma Q., ed. *Greenhouse Gases: Refining the role of carbon dioxide*. Mar. 1998. URL: https://www.giss.nasa.gov/research/briefs/ma_01/.

[18] *Hazardous Substance Data Bank: Nitrogen Dioxide*. URL: https://toxnet.nlm.nih.gov/cgi-bin/sis/search2/r?dbs+hsdb:@term+@rn+10102-44-0ro.

[19] Sillman S. "The relation between ozone, NO_x and hydrocarbons in urban and polluted rural environments". In: *Atmospheric Environemt* 33.12 (1999), pp. 1821–1845.

[20] Turns S.R. *An Introduction to Combustion. Concepts and Applications*. 3rd ed. McGraw-Hill, 2012, pp. 575–576.

[21] Heywood J.B. *Internal Combustion Engine Fundamentals*. McGraw-Hill, 1988, pp. 601–618.

[22] Turns S.R. *An Introduction to Combustion. Concepts and Applications*. 3rd ed. McGraw-Hill, 2012, pp. 593–595.

[23] Heywood J.B. *Internal Combustion Engine Fundamentals*. McGraw-Hill, 1988, pp. 620–625.

[24] *Air Pollution Particulate Matter*. URL: https://www.greenfacts.org/en/particulate-matter-pm/level-2/01-presentation.htm.

[25] Ristovski Z.D. et al. "Respiratory Health Effects of Diesel Particulate Matter". In: *Respirology* (2012).

[26] Bonn WHO Working Group. "Health Aspects of Air Pollution with Particulate Matter, Ozone and Nitrogen Dioxide". In: *World Health Organization Report on a Working Group* (2003).

[27] Editors of Encyclopaedia Britannica. *Nucleation*. URL: https://www.britannica.com/science/nucleation.

[28] *Emissions Standards Reference Guide*. URL: https://www.epa.gov/emission-standards-reference-guide/basic-information-about-emission-standards-reference-guide-road.

[29] *Emissions Standards Reference Guide*. URL: https://www.dieselnet.com/standards/us/hd.php.

[30] Turns S.R. *An Introduction to Combustion. Concepts and Applications*. 3rd ed. McGraw-Hill, 2012, pp. 576–578.

[31] Heywood J.B. *Internal Combustion Engine Fundamentals*. McGraw-Hill, 1988, pp. 626–648.

[32] Turns S.R. *An Introduction to Combustion. Concepts and Applications*. 3rd ed. McGraw-Hill, 2012, pp. 595–597.

[33] Hatch G.E. "Inhalable particles and pulmonary host defense: in vivo and in vitro effects of ambient air and combustion particles". In: *Environmental Research* 36.1 (1985), pp. 67–80.

[34] Brunekreef B. and Forsberg B. "Epidemiological evidence of effects of coarse airborne particles on health". In: *European Respiratory Journal* 26.2 (2010), pp. 309–318.

[35] Schwartz J. and Lucas M.N. "Fine particles are more strongly associated than coarse particles with acute respiratory health effects in schoolchildren". In: *Epidemiology* 11.1 (2000), pp. 6–10.

[36] Hirano S. "Nanoparticles in emissions and atmospheric environment: now and future". In: *Journal of Nanoparticle Research* 5.3-4 (2003), pp. 311–321.

[37] Seaton A. et al. "Particulate air pollution and acute health effects". In: *The Lancet* 345.8943 (1995), pp. 176–178.

[38] Becerra T.A. et al. "Ambient air pollution and autism in Los Angeles County, California". In: *Environmental Health Perspectives* 121.3 (2012), pp. 380–386.

[39] *Emissions Standards Reference Guide*. URL: `https://www.dieselnet.com/standards/eu/ld.php`.

[40] D.B. Kittelson. "Engines and Nanoparticles: A Review". In: *Journal of Aerosol Science* 29.5-6 (1998), pp. 575–588.

[41] D.B. Kittelson. “Driving Down On-Highway Particulate Emissions”. In: *SAE Technical Paper* (2006).

[42] Fino D. et al. “The Role of Suprafacial Oxygen in some Perovskites for the Catalytic Combustion of Soot”. In: *Journal of Catalysts* 217.2 (2003), pp. 367–375.

[43] Russo N. et al. “Studies on the Redox Properties of Chromite Perovskite Catalysts for Soot Combustion”. In: *Journal of Catalysts* 229.2 (2005), pp. 459–469.

[44] Sadakane M. et al. “Facile Procedure To Prepare Three-Dimensionally Ordered Macroporous (3DOM) Perovskite-type Mixed Metal Oxides by Colloidal Crystal Templating Method”. In: *Chemistry of Materials* 17.13 (2005), pp. 3546–3551.

[45] Dhakad M. et al. “Co_3O_4-CeO_2 Mixed Oxide-Based Catalytic Materials For Diesel Soot Oxidation”. In: *Catalysis Today* 132.1–4 (2008), pp. 188–193.

[46] Wagloehner S. and Kureti S. “Study on the mechanism of the oxidation of soot on Fe_2O_3 catalyst”. In: *Applied Catalysis B: Environmental* 125 (2012), pp. 158–165.

[47] Atribak I., Bueno-Lopez A., and Garcia-Garcia A. “Role of Yttrium Loading in the Physico-Chemical Properties and Soot Combustion Activity of Ceria and Ceria-Zirconia Catalysts”. In: *Journal of Molecular Catalysis A: Chemical* 300.1–2 (2009), pp. 103–110.

[48] Krishna K. et al. “Potential Rare Earth Modified CeO_2 Catalysts for Soot Oxidation: I. Characterization and Catalytic Activity with O_2”. In: *Applied Catalysis B: Environmental* 75.3–4 (2007), pp. 189–200.

[49] Obeid E. et al. “Continuously Regenerating Diesel Particulate Filters based on Ionically Conducting Ceramics”. In: *Journal of Catalysts* 309 (2013), pp. 87–96.

[50] Czerwinski J. et al. “Experiences from Nanoparticle Research on Four Gasoline Cars”. In: *SAE Technical Paper* (2015).

[51] Khalek I.A., Bougher T., and Jetter J.J. “Particle Emissions from a 2009 Gasoline Direct Injection Engine using Different Commercially Available Fuels”. In: *SAE Technical Paper* (2010).

[52] De Filippo A. et al. “Particle Number, Size and Mass Emissions of Different Biodiesel Blends vs ULSD from a Small Displacement Automotive Diesel Engine”. In: *SAE Technical Paper* (2011).

[53] Maricq M.M., Szente J.J., and Jahr K. “The Impact of Ethanol Fuel Blends on PM Emissions from a Light-Duty GDI Vehicle”. In: *Aerosol Science and Technology* 46.5 (2012), pp. 576–583.

[54] Peckham M.S. et al. “Study of Particle Number Emissions from a Turbocharged GDI Engine Including Data from a Fast-Response Particle Size Spectrometer”. In: *SAE Technical Paper* (2011).

[55] Myung C.L. and Park S. “Exhaust Nanoparticle Emissions from Internal Combustion Engines: A Review”. In: *International Journal of Automotive Technology* 13.1 (2012), pp. 9–22.

[56] Kirchner U., Vogt R., and M. Maricq. “Investigation of EURO-5/6 Level Particle Number Emissions of European Diesel Light-Duty Vehicles”. In: *SAE Technical Paper* (2010).

[57] Alander T. et al. “Particle Emissions from a Small Two-Stroke Engine: Effects of Fuel, Lubricating Oil, and Exhaust After Treatment on Particle Characteristics”. In: *Aerosol Science and Technology* 39.2 (2005), pp. 151–161.

[58] Christensen A., Westerholm R., and Almen J. “Measurement of Regulated and Unregulated Exhaust Emissions from a Lawn Mower with and without an Oxidizing Catalyst: A Comparison of Two Different Fuels”. In: *Environmental Science and Technology* 35.11 (2001), pp. 2166–2170.

[59] Tanner M., Stryker P., and Brahma I. “Assessment of the feasibility of biodiesel blends for small commercial engines”. In: *ASME Internal Combustion Engine Division Fall Technical Conference* (2012).

[60] Heywood J.B. *Internal Combustion Engine Fundamentals*. McGraw-Hill, 1988, pp. 43–44.

[61] Tazerout M., Le Corre O., and Rousseau S. “TDC Determination in IC Engines Based on the Thermodynamic Analysis of the Temperature-Entropy Diagram”. In: *SAE Technical Paper* (1999).

[62] Pipitone E. and Beccari A. “Determination of TDC in Internal Combustion Engines by a Newly Developed Thermodynamic Approach”. In: *Applied Thermal Engineering* (2009).

[63] Filippo A.D. and Maricq M. “Diesel Nucleation Mode Particles: Semivolatile or Solid?” In: *Environmental Science and Technology* 42.31 (2008), pp. 7957–7962.

[64] Czerwinski J. et al. “Particle Emissions of a TDI-Engine with Different Lubricating Oils”. In: *SAE Technical Paper* (2014).

[65] Lucachick G. et al. “Efficacy of In-Cylinder Control of Particulate Emissions to Meet Current and Future Regulatory Standards”. In: *SAE Technical Paper* (2014).

Appendix A

Engine Specification Sheets

Table A.1: Yanmar diesel CI engine spec sheet.

Specification		Unit	Detail
Engine Model			2004 Yanmar L100EE
Engine Type			Single-cylinder, vertical-4cycle diesel
Cooling System			Forced air cooling by flywheel fan
Combustion System			Direct injection system
Starting System			Starting motor with recoil starter
Number of cylinder-BoreXStroke		mm	1-86-72
Displacement		liters	0.418
Ouput	Continuous	kW(HP)	6.3(8.6)
	Maximum	kW(HP)	7.1(9.6)
Rated engine speed (crankshaft)		rpm	3600
Idle engine speed at no-load high/low		rpm	3780/1200
Compression Ratio			20.0
PTO shaft	PTO Position		Crankshaft
	Direction of rotation		Counterclockwise viewed from PTO
Fuel oil system	Fuel injection pump		Bosch type YANMAR PFE-M type
	Fuel injection timing (FIC: bTDC)	deg	17.0
	Fuel injection nozzle		VCO nozzle Bosch made
	Fuel injection pressure	Mpa (kgf/cm2)	19.6 (200)
Lubricating oil system	Type of lubrication		Forced lubrication via trochoid pump: splash lubrication for valve rocker arm chamber
	Lubricating oil filter		Resin, 60 mesh
	Lubricating oil selection		SAE10W30, API grade CC or higher
	Lubricating oil capacity full/effective	liters	1.65/0.6
Governer			All speed type mechanical
Engine Dimensions (Length X Width X Height)		mm	392 X 470 X 494
Dry Mass		kg	54
Balancer shaft			Single shaft